2021

Solidification Cracking in Binary Al-Cu Alloys Additively Manufactured through Laser Powder Bed Fusion

Keegan Muller

University of Central Florida

SOLIDIFICATION CRACKING IN BINARY AL-CU ALLOYS ADDITIVELY MANUFACTURED THROUGH LASER POWDER BED FUSION

by

KEEGAN MULLER
B.S. University of Central Florida, 2019

A thesis submitted in partial fulfillment of the requirements
for the degree of Master of Science
in the Department of Materials Science and Engineering
in the College of Engineering and Computer Science
at the University of Central Florida
Orlando, Florida

Summer Term
2021

ABSTRACT

Laser Powder Bed Fusion (LPBF) is an additive manufacturing technique with growing relevance in industry. However, alloys with a high susceptibility to micro-cracking during solidification cannot be feasibly manufactured through LPBF, such as in selected high-strength Al-alloys. The cracking susceptibility (CS) of Al-alloys varies with composition, so modeling CS with respect to composition is crucial in designing compatible alloys for LPBF. In a theoretical modeling of solidification cracking based on the Scheil equation, the relative CS is taken as the maximum value of $|dT/df_s^{1/2}|$ when solidification is near completion. However, experimental observations of the crack density in Al-alloys suggest that the composition at which the crack density is maximum occurs at a higher solute concentration than predicted. This shift in the maximum CS can be observed in the theoretical model when a back-diffusion Fourier number was incorporated into the Scheil equation to account for solid-state diffusion during solidification. This shift can also be observed by increasing the partition coefficient above its equilibrium value, which is expected during rapid solidification due to solute trapping. A computational study was conducted on the CS of Al-Cu binary alloys with compositions ranging from 0 to 10 wt.% Cu, in which the Fourier number was varied from 0 to 0.3, and the partition coefficient was varied from its equilibrium value, 0.173, to 0.5. This was then compared to experimental crack density measurements taken for Al-Cu binary alloys with compositions of 1.5, 3, 4.5, 6, and 10 wt.% Cu manufactured through LPBF using gas atomized alloy powders. Increases in Fourier number and/or partition coefficients were both effective in conforming to the experimental results. Increasing the partition coefficient was found to be more effective at shifting the CS towards higher solute concentrations, while increasing the Fourier number was more effective at lowering the magnitude of CS.

The author would like to dedicate this work to his friends, family, and colleagues that have supported him throughout his time at the University of Central Florida and encouraged him to pursue his aspirations.

ACKNOWLEDGMENTS

I would first like to thank my advisor, Dr. Yongho Sohn, for his continuous advice and mentorship throughout the development of my master's thesis. I am incredibly grateful for the opportunities he has given me to conduct research in metal additive manufacturing. My time working with Dr. Sohn has increased my knowledge in this field while improving upon my abilities as a researcher and giving me inspiration for my future career choices. I would also like to thank my thesis committee members, Dr. Akihiro Kushima and Dr. Tengfei Jiang, for their contribution to this thesis.

Additionally, I would like to thank the various colleagues that have trained me, given me guidance, and provided the foundational work for this thesis. This thesis would not have been possible without the assistance of Dr. Le Zhou, Dr. Abhishek Mehta, Dr. Holden Hyer, Dr. Jeongmin Woo, and Mr. Thinh Huynh.

Finally, I would like to thank my family and friends for their support and encouragement in all my endeavors.

TABLE OF CONTENTS

LIST OF FIGURES

LIST OF TABLES

CHAPTER 1 INTRODUCTION

1.1 Background

Laser powder bed fusion (LPBF) is an additive manufacturing (AM) technique to produce metal parts with high complexity and precision. In LPBF, a powder bed is selectively melted to produce 3D parts in a layer-by-layer building process. Initially, a thin layer of powder is distributed onto the build plate using a recoater. Then, the first layer of the part is manufactured by selectively melting the powder with a laser. Upon solidification, the first layer build is complete, and the build plate is lowered by the layer thickness for a new layer of powder to be distributed. The next layer of the part can then be melted by laser and solidified onto the previous layer. This process is repeated until the entire part in 3D is manufactured.

The main limitation of LPBF is that many alloys cannot feasibly be printed without major defects in the microstructure. Three main types of defects that can occur in the microstructure are porosity, lack-of-fusion flaws, and solidification cracking. The formation of these defects is related to energy density, or the amount of energy transferred by laser to the powder bed per unit volume. The energy density is expressed as Equation (1) in terms of the processing parameters of LPBF.

$$Energy\ Density = \frac{Laser\ Power}{Scan\ Speed \times Hatch\ Spacing \times Slice\ Thickness} \quad (1)$$

Since the hatch spacing cannot be adjusted much without the onset of regular porosity and the slice thickness should be as thin as possible to improve the part quality [1], energy density is typically controlled through adjusting the laser power and scan speed. Porosity can occur at high energy densities due to boiling and evaporation, termed keyhole porosity. At low energy densities, lack

of fusion flaws are left behind due to insufficient melting. Therefore, a range of energy density exists in which an alloy can be manufactured with negligible porosity and flaws. Furthermore, solidification cracking will occur below a critical energy density that is dependent on the composition of the alloy being manufactured. For alloys with a high cracking susceptibility, solidification cracking occurs over this entire range of energy densities in which the part can be manufactured with low porosity, resulting in an inability to produce the part without major defects in the microstructure. Therefore, the solidification cracking susceptibility of an alloy is one of the main limitations on determining whether an alloy can successfully be manufactured into a part through LPBF.

Since the cracking susceptibility of an alloy is highly composition-dependent, the composition of industry-relevant alloys can be modified through the gas-atomization of custom powders to better suit LPBF manufacturing. This results in the need for an accurate model to predict an alloy's cracking susceptibility in relation to its composition. Kou [2] was able to successfully model solidification cracking in casting and welding applications by using the Scheil-Gulliver equation to determine the relationship between temperature (T) and fraction solidified (f_s), along with the assumption that the cracking susceptibility is proportional to the maximum value of $\left|dT/df_s^{1/2}\right|$ near complete solidification for an alloy. The Scheil-Gulliver equation is listed as Equation (2), in which T_f is the melting temperature of the solvent, T_L is the liquidus temperature, and k is the partition coefficient.

$$f_s = 1 - \left(\frac{T_f - T}{T_f - T_L}\right)^{\frac{1}{k-1}} \tag{2}$$

However, some of the assumptions of the Scheil-Gulliver equation may not be applicable to LPBF, such as the assumptions that there is no solid-state diffusion [3,4] and that there is local equilibrium at the solid-liquid interface during solidification [5]. It has previously been assumed that there is no solid-state diffusion during solidification due to the very high cooling rates (10^3 - 10^8 K/s) [6] associated with LPBF, but recently it has been suggested by Hyer [3,4] that solid-state diffusion may be significant due to discrepancies between Kou's model and experimental findings. These high cooling rates may also result in rapid solidification where local equilibrium is not achieved, resulting in the partition coefficient taken from the equilibrium phase diagram to potentially be insufficient. Solute trapping can take place during rapid solidification, causing the partition coefficient to increase above its equilibrium value and approach unity [5].

1.2 Motivation

There is a need to better understand solidification cracking in LPBF and how existing cracking susceptibility models can be applied to this manufacturing method. There has been limited research on applying the Scheil-Gulliver equation to solidification cracking for LPBF, and limited work suggests that there is a discrepancy between samples manufactured through LPBF and traditional cracking susceptibility models [3,4]. This would be best examined through binary alloys that are susceptible to solidification cracking, such as Al-Cu, since changes in the alloy's composition would be simple to model and have profound changes in the amount of solidification cracking. Obtaining a better understanding of how solidification cracking can be modeled for LPBF will be useful for designing alloys that can be manufactured without major defects.

1.3 Objective

The aim of this thesis is to model the cracking susceptibility of Al-Cu binary alloys using Kou's cracking criteria with a modified Scheil-Gulliver equation that incorporates solid-state back-diffusion and changes in partition coefficient. The crack density of Al-Cu alloys manufactured through LPBF was experimentally measured so that the composition with the maximum cracking susceptibility from the theoretical model could be compared to the composition at which the crack density was highest experimentally. To examine how solid-state diffusion and rapid solidification may impact the theoretical model, a parametric study was conducted, in which the amount of solid-state diffusion and the partition coefficient were varied in the modified Scheil-Gulliver equation. The composition with the maximum cracking susceptibility index varied significantly with these parameters and was compared to the composition where the maximum cracking density was experimentally observed. Overall, the goal was to model the cracking susceptibility of Al-Cu binary alloys to find which compositions are more resistant to solidification cracking and to gain insight into the solidification cracking mechanics for LPBF.

CHAPTER 2 LITERATURE REVIEW

2.1 Laser Powder Bed Fusion

LPBF is an additive manufacturing method with the capability to produce fully dense parts without the need for molds or special tooling. The main benefit over subtractive manufacturing methods is the ability to adjust part dimensions and print complex parts with little cost or lead time. Currently, LPBF is used in industry to produce small, complex parts that would be difficult to manufacture using traditional manufacturing methods. LPBF is of particular interest even among other additive manufacturing methods due to its high cooling rate and superior surface finish [7]. The part quality produced is dependent on processing parameters and part geometries [8] and the limits of this emerging technology are still being expanded upon. LPBF has the lowest build rate among additive manufacturing methods [9], but as innovation in LPBF systems increase production speed, it is finding its use in industry to produce small, complex parts.

A major limitation of LPBF is that some metal alloys of engineering importance cannot be manufactured without defects. While certain types of defects can be controlled through the processing parameters used in LPBF (laser power, scan speed, hatch spacing, and slice thickness), many alloys have intrinsic limitations that prevent the production of a fully dense part. For example, an alloy must have good flowability in its liquid phase to prevent the formation of pores [10] and must be resilient to solidification cracking due to the high thermal gradient associated with LPBF [11] and large-scale thermal cracking due to residual stresses. The manufactured parts are susceptible to keyhole porosity at high energy densities and incomplete melting, lack of fusion flaws at low energy densities. These types of defects are displayed in Figures 1a and 1b respectively, which are representative micrographs of Al-6 wt.% Cu samples. Keyhole porosity is

a result of gas bubbles getting trapped within the manufactured part and is characterized by smaller, spherical pores [12]. Insufficient melting porosity, termed lack-of-fusion flaw, is due to an insufficient amount of energy being transferred, and typically has larger flaws with a more irregular shape resulting from residual "interparticle space." Defects are a major issue as it lowers the density of the part and impairs the part's mechanical properties by providing a site for stress concentrations. In addition, cracking is a major concern: solidification cracking in the microstructure and large-scale thermal cracking. An example of solidification cracking in the part's microstructure is shown in Figure 1a. Solidification cracking is a result of the shrinkage of grains during solidification and is impacted by the material's ability to "feed" the molten alloy between the grains near the completion of solidification. When the material is unable to have sufficient liquid feeding between the grains, cracking can occur along the grain boundaries to compensate for the reduction in grain volume. Liquid feeding is easier for alloys with a narrow freezing range, so alloy compositions with a narrow freezing range are more resilient to solidification cracking [13]. Additionally, the amount of grain shrinkage is related to the difference in density between the solid and liquid states, so metals with a large density change are more susceptible to solidification cracking [13]. Higher energy densities allow for a greater resistance to solidification cracking, but this is largely dependent on the material's properties as well and can be a major limitation on which alloys are feasible for LPBF manufacturing.

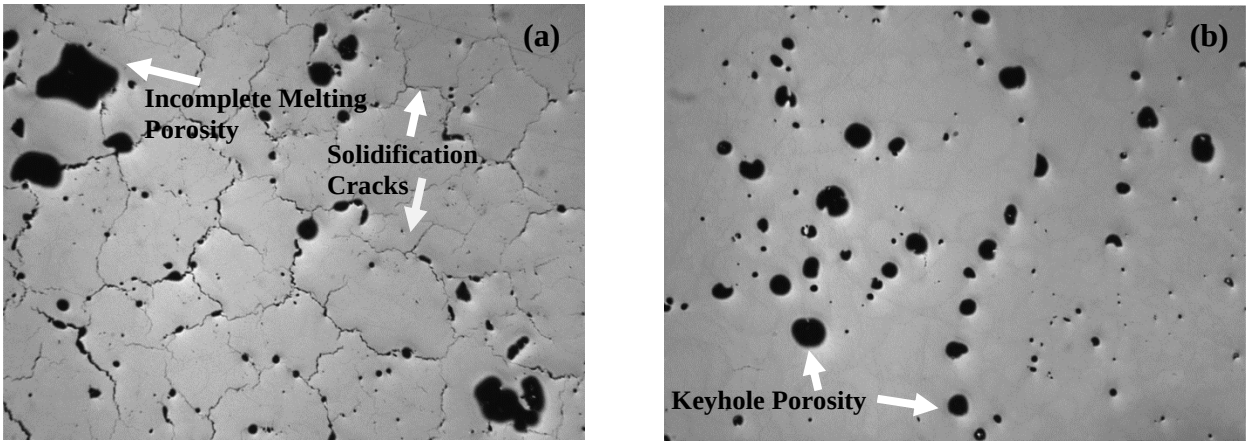

Figure 1. Micrographs of LPBF manufactured Al-Cu (6 Wt.% Cu) samples in the XY plane. (a) Low energy density sample, (b) High energy density sample

Compared to traditional manufacturing methods there is currently less robustness and repeatability for LPBF manufactured parts, because of a greater tendency to form microstructural defects during the part's production [14]. This issue severely limits what alloys can be printed without major defects and loss of physical properties, resulting in high demand for research in the printability of alloys.

2.2 Al-alloys in LPBF

Many commercial Al-alloys have poor compatibility with LPBF because of their tendency to crack during solidification. Al-Si alloys are a notable exception as Si additions have been shown to increase laser absorption, increase the flowability of molten Al, and reduce the thermal contraction during solidification [15]. However, Al-Si alloys do not have the high corrosion resistance, tensile strength, and ductility exhibited by other Al-alloys [16], limiting the applications of LPBF for Al-alloys in industry. High-strength Al-alloys, such as 2xxx, 5xxx, 6xxx, and 7xxx series alloys, are particularly troublesome due to their solidification behavior that yields solidification cracking [16]. These alloys are desirable in many engineering applications due to

their high strength-density ratios [17] and corrosion resistance, so the ability to manufacture complex parts using LPBF would be in high demand for this field if solidification cracking can be mitigated. The 2xxx, 5xxx, 6xxx, and 7xxx series Al-alloys that have been successfully manufactured through LPBF typically required modifications to their composition to increase their resistance to cracking, emphasizing the importance of alloy composition on printability.

The cracking susceptibility of Al-Cu binary alloys, which forms the basis of 2xxx series Al-alloys, was investigated in this thesis. These alloys were chosen due to the expectation of composition-dependent solidification cracking. The objective of this thesis is to compare the experimental crack density of LPBF manufactured samples to cracking susceptibility models used in casting and welding manufacturing, so having samples with a large amount of cracking that varies significantly with composition is ideal. Due to their high susceptibility to cracking, 2xxx series Al-alloys based on the binary Al-Cu system are not considered "printable" but being able to quantify these cracks makes this alloy an ideal candidate to be studied in this thesis.

While most Al-Cu-based alloys are not considered printable using LPBF, there has been some success in manufacturing modified Al-Cu alloys. Al-Cu-Sc-Zr [16,18] and Al-Cu-TiB_2 [19] have been successfully manufactured through LPBF. The addition of Sc and Zr has been found to reduce the solidification cracking susceptibility of other Al-alloys as well, including 5xxx Al-Mg alloys [20,21], 6xxx Al-Mg-Si alloys [22,23], and 7xxx Al-Zn alloys [24]. This is believed to reduce solidification cracking through the primary formation of Al_3Sc and Al_3Zr precipitates that act as heterogeneous nucleation sites [21,22,24], which reduce the grain size of the solidification microstructure. Similarly, the addition of TiB_2 to reduce cracking susceptibility is not exclusive to 2xxx series alloys, with TiB_2 being an effective grain refiner for Al-alloys in general [19]. These grain refinement methods aid in increasing the printability of Al-alloys, but the aim of this work

is to investigate how adjusting the composition of the base alloys impacts the cracking susceptibility. When designing an Al-alloy that can be manufactured successfully through LPBF, the addition of Sc, Zr, or TiB_2 will help reduce cracking, but the ratio of Al to its primary alloying element must also be considered.

2.3 Modeling Solidification Cracking

There has been little research into the application of traditional models for cracking susceptibility in casting and welding applications to LPBF. Since the ratio of Al to its primary alloying element impacts its susceptibility to cracking, which is the main limitation of manufacturing Al-alloys with LPBF, being able to successfully model solidification cracking susceptibility in terms of composition is essential in designing compatible Al-alloys. For solidification cracking during casting and welding, Kou [2] suggested that crack initiation is proportional to $\left|dT/df_s^{1/2}\right|$ near complete solidification, which he defined as the cracking susceptibility index. This is based on the idea that sufficient liquid must be fed to the grain boundaries through back-filling to prevent cracking as the grains shrink during solidification. When $\left|dT/df_s^{1/2}\right|$ is large, more cracks will be able to initiate due to a reduction in liquid feeding and slower grain growth allowing for more time for cracks to initiate. This model matched experimental findings for Al-alloys in casting and welding applications. In Kou's study, the relation between T and f_s was obtained from the Scheil-Gulliver equation but this methodology can be improved upon. A major limitation of the Scheil-Gulliver equation is that it assumes that there is diffusion only in the liquid phase during solidification. Hence, several modifications to the Scheil-Gulliver equation have been developed to incorporate back-diffusion into the relationship

between T and f_s, including the Brody-Flemings model [25], the Clyne-Kurz model [26], and the Kobayashi-Ohnaka model [27], which are listed as Equations (3), (4), and (5), respectively.

$$f_s = \frac{1}{1-2\alpha k}\left[1-\left(\frac{T_f - T}{T_f - T_L}\right)^{\frac{1-2\alpha k}{k-1}}\right] \quad (3)$$

$$f_s = \frac{1}{1-2\Omega k}\left[1-\left(\frac{T_f - T}{T_f - T_L}\right)^{\frac{1-2\Omega k}{k-1}}\right] \quad (4)$$

$$f_s = \frac{1+2\alpha}{1+2\alpha-2\alpha k}\left[1-\left(\frac{T_f - T}{T_f - T_L}\right)^{\frac{1}{\eta}}\right] \quad (5)$$

In Equation (3), (4), and (5), T and f_s are variable while T_f, T_L, and k are constants that are dependent on the alloy composition being manufactured. T_f, T_L, and k are obtainable for all alloy compositions from the equilibrium phase diagram if local equilibrium is assumed at the liquid-solid interface, but some calculation is required to obtain k. The partition coefficient, k, is defined as the ratio of solute concentration in the solid and liquid states for the alloy, which are C_S and C_L respectively. While the partition coefficient is composition-dependent, it is typically simplified when utilizing modified forms of the Scheil-Gulliver equation by approximating the solidus and liquidus as straight lines, so that k can be calculated using Equation (6) regardless of composition. The Brody-Flemings model was the first modification of the Scheil-Gulliver equation to introduce a back-diffusion parameter to account for solid-state diffusion during solidification, while the Clyne-Kurz and Kobayashi-Ohnaka models made minor improvements upon the equation developed by Brody-Flemings [28].

In the Brody-Flemings model, α is the back-diffusion Fourier number, which is a flux term associated with solid-state back-diffusion during solidification. While α is dependent on alloy composition and processing parameters, it is typically approximated as a constant for the sake of

simplicity. Mathematically, α can be solved by using Equation (7). In this equation, D_s is the solid-state diffusion coefficient during solidification, t_f is the freezing time, and L is the characteristic length. For solidification, L is taken as half of the secondary dendrite arm spacing (SDAS). The Clyne-Kurz model is very similar to the Brody-Flemings model but modifies the α parameter to limit errors that occur due to geometrical simplifications when is α large [26]. The Ω term that replaces α in the Brody-Flemings model can be calculated from α using Equation (8). Ω is nearly equivalent to α for low values of α, but as α approaches 0.5 and above, Ω will be significantly smaller than α. While the Kobayashi-Ohnaka model does not incorporate this geometric factor, it improves upon the Brody-Flemings model by incorporating an additional thermal model for solidification into the equation's derivation that accounts for multi-component alloys, variable diffusion coefficients as temperature changes during solidification, and an estimation of the diffusion path [27]. In this model, η is a constant defined by Equation (9) which can be solved from k and α. The Clyne-Kurz and Kobayashi-Ohnaka models are the most rigorous, so either of them would be preferable to use when finding a relationship between T and f_s. These modified Scheil-Gulliver equations allow for a relationship between composition and cracking susceptibility to be developed using Kou's cracking criteria that incorporates the potential for solid-state diffusion during solidification.

$$k = \frac{C_S}{C_L} \tag{6}$$

$$\alpha = \frac{D_S t_f}{L^2} \tag{7}$$

$$\Omega = \alpha\left(1 - e^{-\frac{1}{\alpha}}\right) - \frac{1}{2}e^{-\frac{1}{2\alpha}} \tag{8}$$

$$\eta = \frac{(k-1)(1+2\alpha)}{1+2\alpha-2\alpha k} \tag{9}$$

While Kou's method of modeling solidification cracking matched experimental data for casting and welding applications in Al-alloys, their application to LPBF has not been extensively investigated and initial investigations show some discrepancies with experimental results. While it would be expected that back-diffusion is negligible due to the high cooling rates associated with LPBF, Hyer [3,4] found that Kou's cracking criteria only matched experimental results when a certain amount of back-diffusion during solidification was included. When solid-state diffusion coefficients reported in literature were incorporated to calculate the back-diffusion Fourier number for Al-Si [3,4] and Al-Mg (AA5083) [3], the composition with the maximum cracking susceptibility was at a lower solute concentration than experimentally observed. When the amount of solid-state diffusion was increased above its reported value, the composition with the maximum cracking susceptibility shifted to higher solute concentrations. These results suggest that the solid-state diffusion coefficient during solidification may be higher than literature values for LPBF by several orders of magnitude. One explanation is that since the solid is surrounded by the liquid melt during solidification, the diffusion coefficient may significantly increase. However, since there was not much cracking observed in the Al-Si alloys and cracking susceptibility is not very compositionally dependent for these alloys, it was determined that further research was needed to confirm that the results were not caused by experimental uncertainty. While the variation in crack density was more pronounced in the investigation of Al-Mg binary alloys, only a few Mg concentrations were tested with concentrations too low to observe a peak in crack density, so an extended study would be required to have meaningful results.

Aside from using Kou's cracking criteria to predict cracking susceptibility, there has been some limited success in modeling cracking susceptibility using alternative methods for LPBF. A study by Hu [29] used a similar method to Kou's cracking criteria to develop a model that predicts solidification cracking behavior for LPBF manufacturing based on processing parameters. Like Kou's cracking criteria, this model is also based on the assumption that cracking takes place in the mushy zone between solidifying grains when there is insufficient liquid feeding near the completion of solidification. The main impact that processing parameters have on the cracking susceptibility is through the cooling rate, as faster cooling rates do not provide as much time for liquid feeding to occur. This was incorporated into their model through the Rosenthal equation to incorporate the impact of processing parameters. Through this, they were able to define a critical scan speed, above which solidification cracking will occur. This critical scan speed is dependent on alloy composition as well through the solidification range and the alloy's thermal properties. It was found that in the modeling of Al-Cu alloys, cracking initiated at the lowest scan speed for 4 wt.% Cu alloy when composition-dependent thermal and physical properties were taken into consideration, which more closely matched experimental findings than the composition most susceptible to cracking being 1 wt.% Cu predicted based on solidification ranges alone. While this model requires a more extensive understanding of how the alloy's thermal properties vary with changing composition, this method may be more robust than Kou's cracking criteria and provides additional insight into solidification cracking behavior. While Kou's cracking criteria will be the primary focus of this work since its simplicity will allow it to be used more readily across different applications, the model developed by Hu is a viable alternative that would also give insight into the ideal alloy compositions and processing parameters needed for a fully dense print.

2.4 Rapid Solidification and the Partition Coefficient

While Hyer [3,4] suggests that the discrepancy in cracking susceptibility between Kou's cracking criteria and experimental results may be due to the solid-state diffusion coefficient being higher than literature values, another possibility is the partition coefficient being larger than its equilibrium value. An underlying assumption of the Scheil-Gulliver equation and its modified forms is that the partition coefficient is taken from the alloy's equilibrium phase diagram with the solidus and liquidus approximated as straight lines [28]. This leads to a constant partition coefficient that is representative of most alloy compositions. However, this assumption may not hold for LPBF due to rapid solidification due to high cooling rates. During rapid solidification, local equilibrium at the solid-liquid interface would not be achieved, resulting in solute trapping and potentially the development of metastable phases [5]. As the velocity of the solid-liquid interface increases, these effects become more pronounced since the solute does not have time to diffuse across the solid-liquid interface and is trapped within the solid-state. This implies that at high cooling rates where the velocity of the solid-liquid interface is high, the partition coefficient will approach 1, as the solute concentration in the solid and liquid phases will be more similar when solute trapping occurs. Since the equilibrium value of the partition coefficient is < 1 for aluminum binary alloys, it is expected that the partition coefficient is higher when these alloys are manufactured through LPBF compared to traditional manufacturing methods.

The partition coefficient being above its equilibrium value for Al-alloys manufactured through LPBF has been observed experimentally. Qin [30] analyzed the microstructure of eutectic and hypoeutectic AlSi10Mg manufactured through LPBF and found evidence of solute trapping. They observed a higher solubility limit in the α-Al phase than the equilibrium value, which is indicative of solute trapping. This would correspond to an increase in the partition coefficient, and

hence a shift in the predicted cracking susceptibility curve towards higher solute concentrations. Ghoncheh [31] found that the partition coefficient was greater than its equilibrium value in an A205 alloy manufactured through LPBF. They attributed this to a high solid-liquid interface velocity and natural convection during solidification. Since a high solid-liquid interface velocity would result in solute trapping, this further confirms that the partition coefficient is increasing due to this mechanism. Based on these findings, calculating the partition coefficient from the equilibrium phase diagram may give an underestimation of its true value due to rapid solidification occurring in LPBF.

CHAPTER 3 EXPERIMENTAL METHODOLOGY

3.1 Fabrication of Samples

3.1.1 Manufacturing of Powders

Al-Cu binary alloy powders with compositions of 1.5, 3, 4.5, 6, and 10 wt.% Cu were manufactured through gas atomization. In powder manufacturing, atomization and reduction processes are viable for producing large amounts of metal powders, but atomization methods are more commonly used. This is because atomization allows for more control over the resulting powder's characteristics, such as powder size, without compromising the morphology of the powder [32]. Additionally, atomization is useful for creating powders with a range of compositions, since metal charges can be mixed in their molten form during the atomization process. Atomization manufacturing techniques for powder production are typically used for LPBF applications, since the powder used in LPBF must be small, spherical, and have good flowability. Gas atomization is the most widely used atomization method, which uses high-pressure gas streams to break a molten liquid stream into droplets while also quenching the resulting particles. A diagram that demonstrates the gas atomization procedure used is shown in Figure 2. Metal charges are initially melted in a melting crucible, and the molten liquid is transferred to a holding crucible, called tundish. This holding crucible is maintained at a constant temperature as the molten liquid is ejected into a chamber by gravity with a pressurized gas stream. This gas stream breaks up the molten liquid into droplets while rapidly cooling it, producing small, spherical powders. The properties of the powders produced can be optimized by manipulating the induction temperature used to melt the metal charges, the holding temperature of the crucible, the diameter of the nozzle, and the pressure of the gas stream.

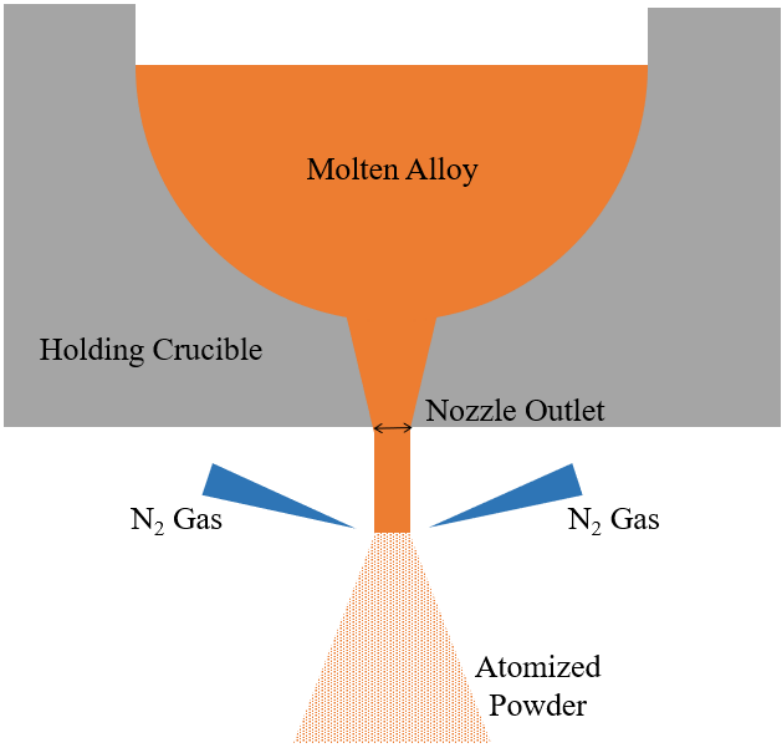

Figure 2. Gas atomization schematic

To manufacture the various Al-Cu alloys, pre-alloyed Al50Cu charges were weight saturated with pure aluminum charges until the desired composition was obtained. These charges were heated in a melting crucible at 950 °C and poured into a holding crucible held at 850 to 950 °C. The molten metal exited this holding crucible through a nozzle with a diameter of 3 to 3.5 mm. Pressurized nitrogen gas at 2 to 3 MPa was used to break up the molten stream into small droplets, forming powders as they solidify. The apparatus used for the gas atomization of the Al-Cu alloys is shown in Figure 3. Additionally, a full list of the processing parameters used in the successful atomization runs of each alloy is listed in Table 1. After gas atomization, the powders were sieved to limit the maximum powder diameter to 75 μm.

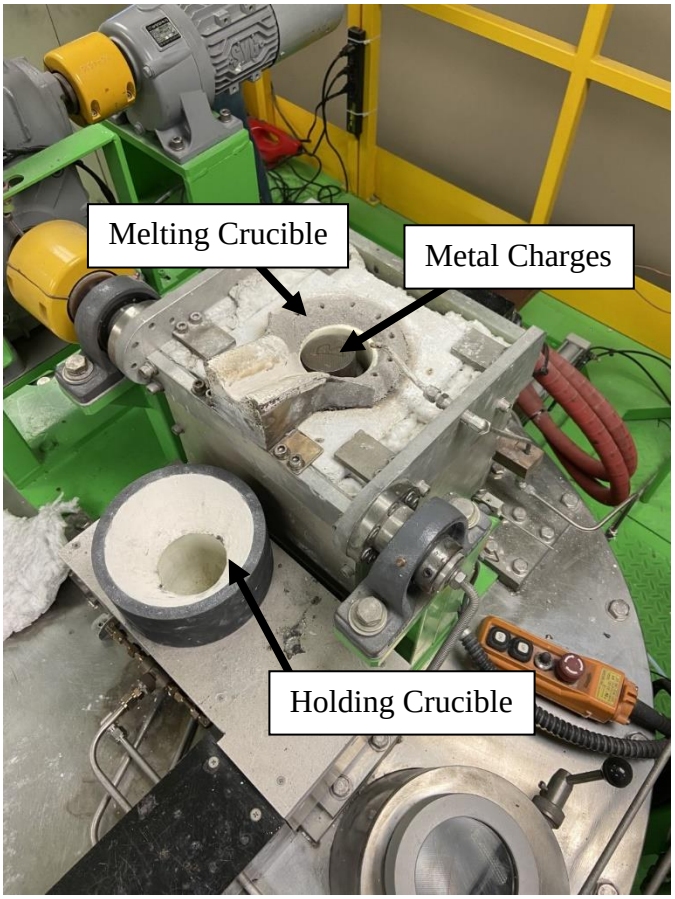

Figure 3. Gas Atomization Apparatus

Table 1. Processing Parameters used for Gas Atomization

Composition (wt.%)	Pressure (MPa)	Induction Temp. (°C)	Hold Temp. (°C)	Nozzle Diameter (mm)
Al1.5Cu	2.1	950	950	3.5
Al3Cu	2.1	950	950	3
Al4.5Cu	2 - 3	950	950	3
Al6Cu	3	950	950	3
Al10Cu	2.5 - 3	950	850	3

3.1.2 LPBF Processing

Cuboidal samples with dimensions of 10 x 10 x 10 mm were manufactured using an SLM 125 HL LPBF system equipped with a Ytterbium fiber laser that has a 70 μm spot size and 1070 nm wavelength. A photograph of the SLM 125 HL LPBF system is shown in Figure 4. The 125 HL LPBF system has a maximum build volume of 125 x 125 x 125 mm, and a build rate of up to 25 cm^3/h. All builds were performed in an inert N_2 atmosphere with an O_2 concentration of less than 0.2%, and onto a heated substrate at 100°C. A stripe scan pattern was used for all builds. Samples at each composition were printed using 15 different operating parameters, which are listed in Table 2. The energy density corresponding to the processing parameters for each sample was calculated using Equation (1), and are listed in Table 2. Henceforth, individual samples will be denoted as AlXCu_S# where X is the wt.% Cu and # is the sample number based on the processing parameters listed in Table 2. For example, the 4.5 wt.% Cu sample manufactured at 200 W laser power and 100 mm/s scan speed will be denoted as Al4.5Cu_S1.

Figure 4. Image of the SLM 125 HL LPBF system

Table 2. LPBF Parameters

Sample Number	Laser Power (W)	Scan Speed (mm/s)	Hatch Spacing (µm)	Slice Thickness (µm)	Scan Rotation (°)	Energy Density (J/mm^3)
1	200	100	130	30	67	512.8
2		200				256.4
3		300				170.9
4		400				128.2
5		600				85.5
6		800				64.1
7		1000				51.3
8	350	400				224.4
9		600				149.6
10		800				112.2
11		1000				89.7
12		1200				74.8
13		1400				64.1
14		1600				56.1
15		1800				49.9

After the samples were fabricated, they were removed using an oscillating multi-tool. Cross-sectional slices were taken parallel to the build direction (XZ plane) and normal to the build direction (XY plane), as depicted by Figure 5. The cross-sectional slices were mounted in epoxy resin and mechanically polished using SiC papers down to 1 µm, then to 0.05 µm using colloidal silica.

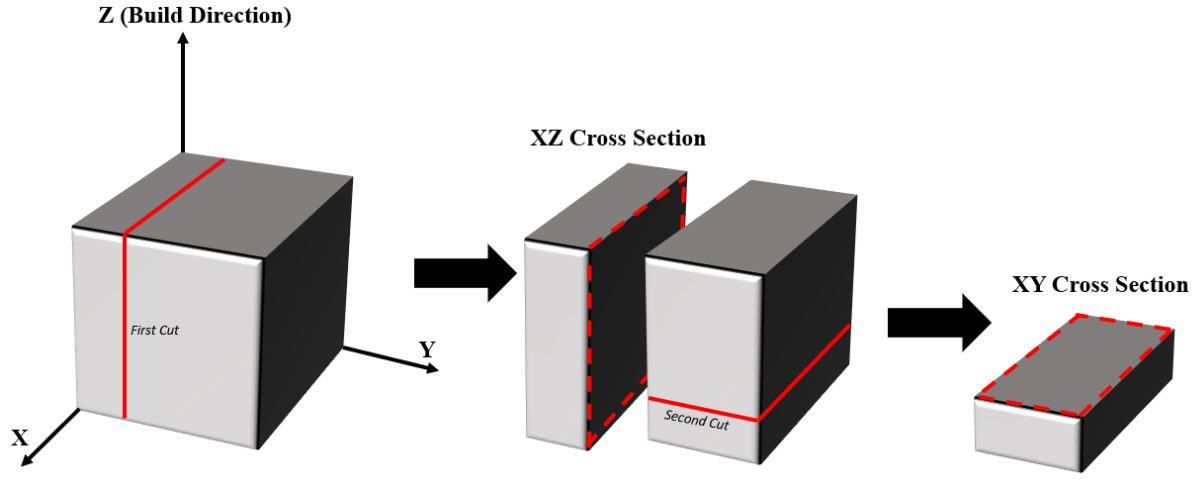

Figure 5. Cross-Section Schematic

3.2 Crack Density Analysis

The microstructure of the samples was observed under an optical microscope. Four micrographs were taken at 5X magnification in representative locations within the sample for the XY and XZ cross-sections. An image of a calibration slide was also taken at the same magnification. ImageJ was then used to quantify the crack density of the samples from these micrographs using Equation (10). In this equation, ρ_C is the crack density, L_C is the length of the crack, and A is the area being observed. After ImageJ was calibrated using the image of the calibration slide, the cracks were manually outlined in ImageJ and the length of each crack was measured. Figure 6 demonstrates how these measurements were carried out, with the yellow lines being the manually highlighted cracks. After taking these measurements across the four micrographs of each sample and cross-section, average crack densities were calculated for each sample.

$$\rho_C = \frac{\sum L_C}{A} \tag{10}$$

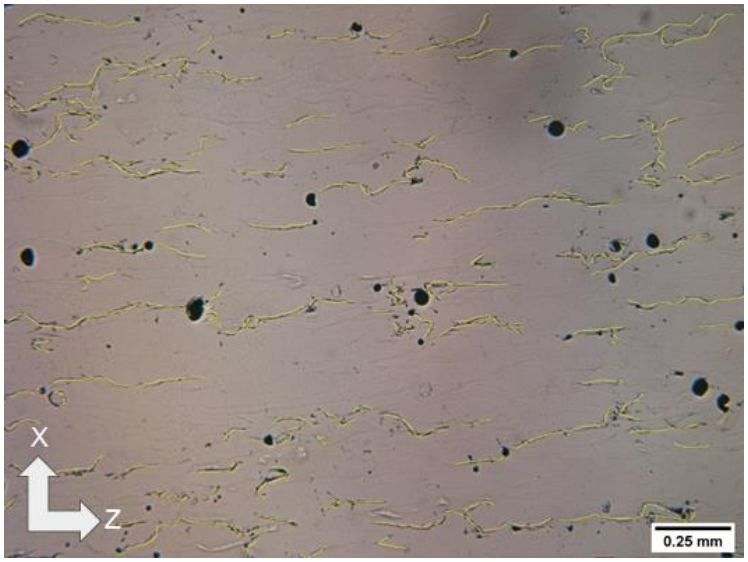

Figure 6. Representative micrograph highlighting the cracks in Al4.5Cu_S12 in the XZ plane

3.3 Modeling Cracking Susceptibility

The first step in modeling cracking susceptibility for Al-Cu alloys was the creation of temperature vs. fraction solidified curves for various alloy compositions. To account for back-diffusion, the modified Scheil equation developed by Clyne and Kurz was used. The Kobayashi-Ohnaka model is also a viable alternative that accounts for solid-state back-diffusion, but the Clyne-Kurz model was chosen since high values for the back-diffusion Fourier number will be considered. The Clyne-Kurz model is better suited for applications where α is high so it was chosen in this analysis, but both models would give similar results. The constants T_f and T_L were taken directly from the equilibrium phase diagram for Al-Cu. Initially, the equilibrium value for the partition coefficient was considered, so the equilibrium phase diagram was used in its calculation. The liquidus and solid lines were approximated as straight lines so that k remains constant regardless of composition in the hypoeutectic region and so that Equation (6) is applicable. It was also assumed that α was a constant independent of composition for the sake of simplification, which is another common assumption used in variations of the Scheil equation for simplicity [28]. The temperature range over which the Clyne-Kurz model was used to find the relationship between T and f_s was from the liquidus temperature, which is the temperature at which solidification initiates, to the eutectic temperature. Since Kou defined the cracking susceptibility index as $\left|dT/df_s^{1/2}\right|$, and the Clyne-Kurz model defines the relationship between T and f_s, the relation between T and $f_s^{1/2}$ was derived from Equation (4), expressed as:

$$f_s^{1/2} = \sqrt{\frac{1}{1-2\Omega k}\left[1-\left(\frac{T_f-T}{T_f-T_L}\right)^{\frac{1-2\Omega k}{k-1}}\right]} \tag{11}$$

The crack susceptibility index was defined by Kou (2) as the maximum value of $\left|dT/df_s^{1/2}\right|$ near complete solidification ($0.9 < f_s < 0.99$). The solidification range of $0.9 < fs < 0.99$ is chosen to fall within the "mushy zone" between grains during solidification inside which cracking can occur [33]. The lower bound is somewhat arbitrary as the maximum value of $\left|dT/df_s^{1/2}\right|$ will always be higher at larger values of f_s, but the upper bound is a fixed cutoff which would significantly alter the results if an inappropriate value were chosen. This upper boundary represents the transition of the "mushy zone" to a fully solid-state in which solidification cracking will not initiate. The upper bound can be taken as 0.98 [29, 33] or 0.99 [2], but reducing the upper bound below 0.98 even slightly can greatly impact the results. For example, Kou attempted to change the upper bound to 0.94 to observe how the results were impacted, and the cracking susceptibility curve shifted significantly towards higher solute concentrations [2]. For the purposes of this analysis, the solidification range over which the slope was calculated was taken to be $0.8 < f_s < 0.99$. This range was chosen since some compositions did not reach $f_s = 0.9$ before their eutectic temperature was reached, so the lower bound of the solidification range was reduced to obtain meaningful data. Since Equation (11) is composition-dependent through T_L, the cracking susceptibility index was calculated for compositions from 0 to 10 wt.% Cu with increments of 0.5 wt.%. This was done by plotting the relationship between $f_s^{1/2}$ and T at constant compositions and determining the maximum slope over $0.8 < f_s < 0.99$. Each composition produces a unique $f_s^{1/2}$ vs T curve, giving a value for cracking susceptibility index at each alloy composition. Using this, a plot of cracking susceptibility index vs. composition was generated to be compared with the experimental data. It was initially observed that the composition with the highest cracking susceptibility index was at a significantly lower solute concentration than experimentally observed, which matched the findings by Hyer [4] on Al-Si binary alloys.

Since the experimental data indicated that a shift in the cracking susceptibility curve towards higher solute concentrations was necessary to match the experimental data, it was believed that either the "effective" solid-state diffusion coefficient was higher than its literature value, which would increase the value of α, or that the partition coefficient was higher than its equilibrium value due to rapid solidification. Hence, a parametric study was conducted on α and k to observe the impact of changing these variables on the cracking susceptibility curve. In the parametric study, α was varied from 0 to 0.3 in increments of 0.05, while k was taken as its equilibrium value of 0.173 and varied between 0.2 to 0.5 in increments of 0.1. At each pair of α and k values, curves for the cracking susceptibility index in terms of alloy composition were generated using the aforementioned methodology. A major point of interest in this parametric study was observing which composition will have the highest cracking susceptibility index at different values of α and k, as this was compared to where the maximum crack density was observed experimentally. Hence, an expansion on the parametric study was also conducted in which k was varied from 0.175 - 0.475 in increments of 0.025, and the value of α was iteratively determined that corresponded to a peak crack susceptibility index at the same composition that was observed to have the highest crack density experimentally. This was done to develop an equation to approximate the relationship between α and k required to match the experimental results so that if one variable is known, the other can be solved for. Finally, existing literature on the rapid solidification of Al-Cu alloys manufactured through LPBF was used to obtain a general idea of how much k should increase above its equilibrium value. The developed relationship between α and k was utilized to determine which variable was primarily responsible for the experimentally observed shift in the cracking susceptibility towards higher solute concentrations.

CHAPTER 4 RESULTS AND DISCUSSION

4.1 Experimental Findings

The crack densities of hypoeutectic Al-Cu binary alloys with compositions of 1.5, 3, 4.5, 6, and 10 Wt.% Cu were investigated across various processing parameters. Samples at each composition were manufactured at scan speeds ranging from 100 mm/s to 1000 mm/s at a laser power of 200W, and scan speeds from 400 to 1800 mm/s at a laser power of 350W. This provided samples at each composition with a variety of energy densities. The hatch spacing and slice thickness were held constant at 130 μm and 30 μm, respectively. As such, the energy densities were calculated for each set of processing parameters, which ranged from 49.9 J/mm^3 to 512.8 J/mm^3. A list of sample numbers and their corresponding processing parameters can be found in Table 2. For each sample, cross-sections of the XY plane and the XZ plane were taken, which were normal to and along the build direction, respectively. Four micrographs were taken of each plane in every manufactured sample for crack density analysis and to observe the samples' microstructures. The microstructures of the manufactured samples are presented in Figure 7.

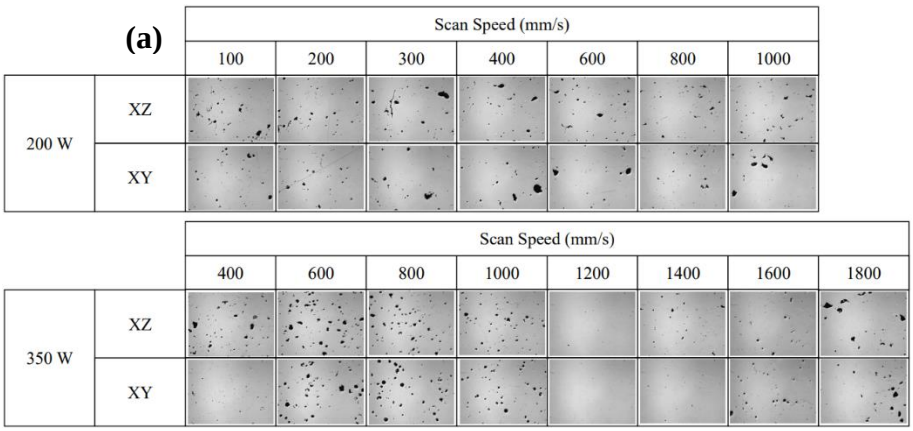

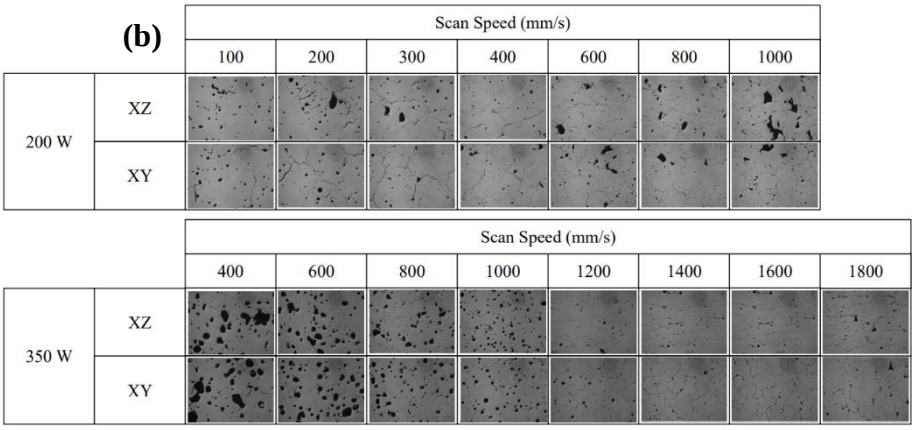
(b)
Scan Speed (mm/s)
100
200
300
400
600
800
1000
200 W
XZ
XY
Scan Speed (mm/s)
400
600
800
1000
1200
1400
1600
1800
350 W
XZ
XY

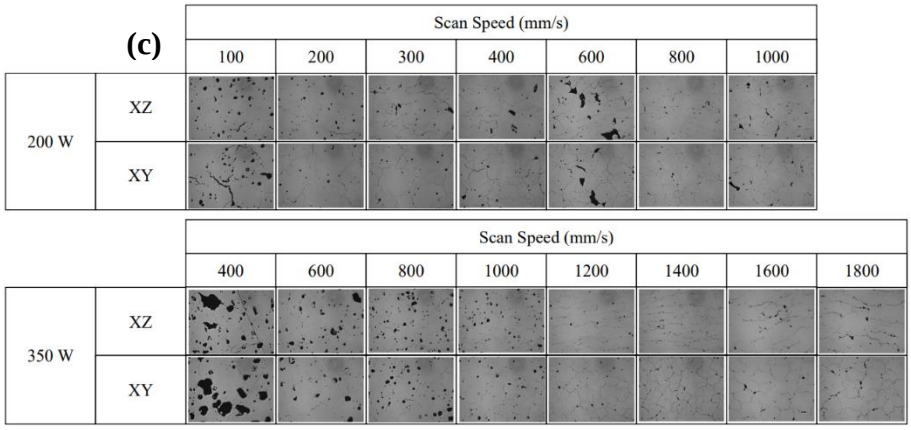
(c)
Scan Speed (mm/s)
100
200
300
400
600
800
1000
200 W
XZ
XY
Scan Speed (mm/s)
400
600
800
1000
1200
1400
1600
1800
350 W
XZ
XY

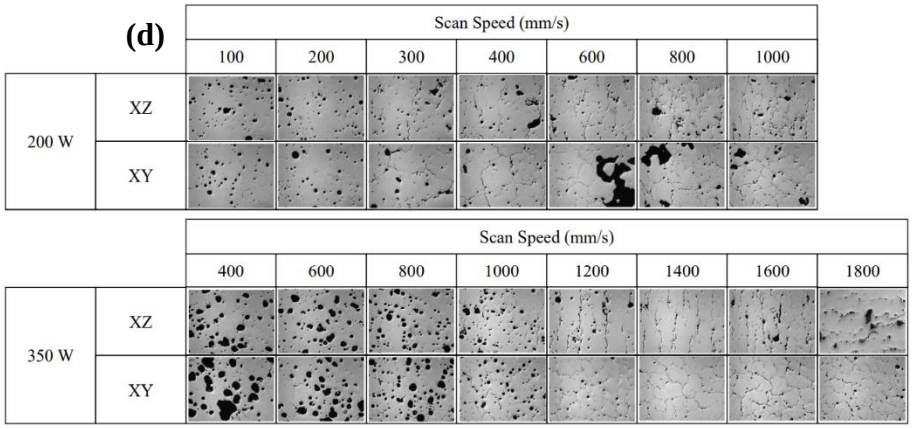
(d)
Scan Speed (mm/s)
100
200
300
400
600
800
1000
200 W
XZ
XY
Scan Speed (mm/s)
400
600
800
1000
1200
1400
1600
1800
350 W
XZ
XY

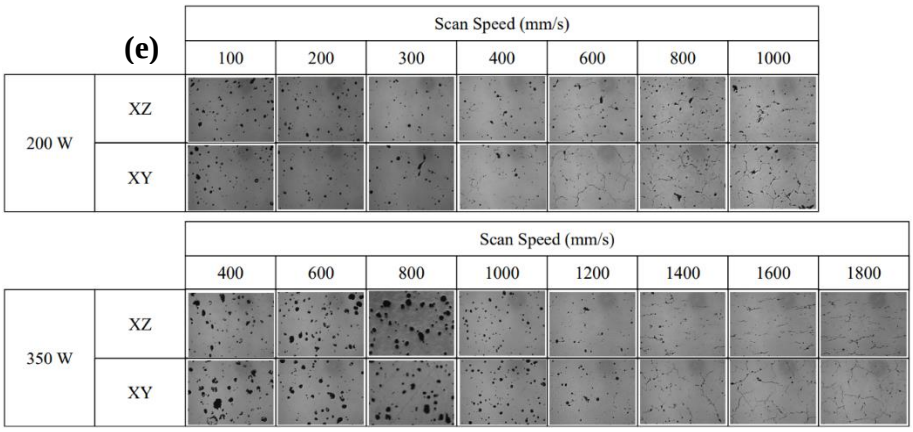

Figure 7. Micrographs of manufactured Al-Cu alloys for all processing parameters and compositions. (a) Al1.5Cu, (b) Al3Cu, (c) Al4.5Cu, (d) Al6Cu, (e) Al10Cu

Initial observations suggest that there was little cracking in the Al1.5Cu samples regardless of processing parameters. For the other compositions, there appears to be a significant increase in the amount of cracking with increasing scan speed, which is expected. At high scan speeds (low energy densities), the cooling rate during solidification is high and alloys become more susceptible to solidification cracking. For alloys manufactured through LPBF, there is a minimum energy density required to avoid solidification cracking, and crack density is expected to increase as the energy density is further reduced below this critical value. The was a noticeable difference in the appearance of cracks when comparing the XY and XZ planes. In the XY plane, the cracks were more interconnected and formed circular structures. In the XZ plane, the cracks were less connected and more linear in shape. This can be attributed to the orientation of the grains in samples produced by LPBF. Since grain boundaries provide pathways for cracks to propagate and solidification cracking initiates at the mushy zone between grains, the cracking structure in the microstructure of the samples will be reflective of the grain boundaries in each plane.

Micrographs in Figure 7 also exhibit both keyhole porosity and insufficient melting porosity. Keyhole porosity is the formation of pores due to boiling/evaporation at high energy

densities due to an excess of energy being transmitted by the laser to the melt pools. At low energy densities, lack of fusion flaws are expected to form due to insufficient melting from the laser not transmitting enough power to the melt the powders. From Figure 7, there is significantly more porosity at very high and very low energy densities, which is consistent with the expected observations. The main observation from the microstructure that deviates from initial expectations is the lack of cracking for the Al1.5Cu samples, shown in Figure 7a. Analysis of the hot tearing tendencies for Al-Cu binary alloys suggests that the composition with the highest susceptibility to solidification cracking is around 1 wt.% Cu [34], with cracking susceptibility decreasing when the solute concentration is further increased. Based on this, it would be expected that the Al1.5Cu samples would have the most amount of cracking, which is the opposite of what initial observations of the microstructure suggest. However, recent findings by Hyer et al. [3,4] and Hu et al. [29] suggest that for alloys manufactured through LPBF, the composition at which the maximum cracking susceptibility occurs is at a higher solute concentration than when the alloy is manufactured through traditional manufacturing methods. The lack of cracking observed for the Al1.5Cu samples supports this potential shift in maximum cracking composition and will be the main point of investigation for this thesis.

The crack density was quantified across all samples in the XY and XZ planes. To do so, four micrographs were taken of each plane for every sample and the crack density was determined based on Equation (10). The length of the cracks for each image was measured through image analysis utilizing ImageJ. Calibration was necessary to relate crack length in pixels to its actual length and determine the area of the micrographs, so a micrograph was taken of a calibration slide at the same magnification for this purpose. The crack densities were then averaged across the four micrographs and the error was taken as the standard deviation. The only exception to this is

Al1.5Cu_S1 since only one micrograph was obtained for the XY and XZ planes of the sample, and hence a standard deviation was not obtained. The average crack densities and standard deviations are tabulated in Table 3.

Table 3. Crack density measurements for Al-Cu samples manufactured through LPBF. The units of crack density are 1/mm and the error is taken as the standard deviation.

	1.5 Wt% Cu		**3 Wt% Cu**		**4.5 Wt% Cu**		**6 Wt% Cu**		**10 Wt% Cu**	
Sample	XZ	XY	XZ	XY	XZ	XY	XZ	XY	XZ	XY
1	0.011	0.094	0.502 ± 0.316	0.519 ± 0.236	0.229 ± 0.229	0.669 ± 0.303	0.036 ± 0.035	0.057 ± 0.041	0.030 ± 0.014	0.016 ± 0.020
2	0.153 ± 0.064	0.137 ± 0.050	1.413 ± 0.232	1.956 ± 0.265	1.686 ± 0.271	2.226 ± 0.260	0.170 ± 0.068	0.423 ± 0.230	0.114 ± 0.054	0.269 ± 0.250
3	0.138 ± 0.053	0.106 ± 0.035	2.522 ± 0.419	3.197 ± 0.339	2.765 ± 0.106	4.104 ± 0.221	0.658 ± 0.120	1.826 ± 0.312	0.431 ± 0.065	0.650 ± 0.253
4	0.271 ± 0.153	0.091 ± 0.035	2.805 ± 0.250	4.230 ± 0.226	3.383 ± 0.567	4.552 ± 0.382	1.181 ± 0.062	2.456 ± 0.350	0.603 ± 0.068	0.787 ± 0.186
5	0.161 ± 0.233	0.163 ± 0.050	4.276 ± 0.280	4.714 ± 0.344	3.531 ± 0.441	4.654 ± 0.279	1.242 ± 0.299	2.687 ± 0.459	0.975 ± 0.114	2.339 ± 0.523
6	0.168 ± 0.065	0.092 ± 0.036	4.550 ± 0.242	5.407 ± 0.290	3.880 ± 0.419	4.210 ± 0.493	2.307 ± 0.276	4.150 ± 0.415	1.067 ± 0.440	2.409 ± 0.218
7	0.315 ± 0.117	0.242 ± 0.103	4.611 ± 0.666	5.425 ± 0.589	3.175 ± 0.467	4.365 ± 0.319	2.306 ± 0.569	3.774 ± 0.464	1.110 ± 0.201	2.566 ± 0.099
8	0.031 ± 0.037	0.048 ± 0.032	0.490 ± 0.122	0.697 ± 0.293	0.313 ± 0.106	0.365 ± 0.052	0.084 ± 0.030	0.129 ± 0.075	0.057 ± 0.045	0.071 ± 0.020
9	0.048 ± 0.052	0.101 ± 0.060	0.440 ± 0.186	0.776 ± 0.359	0.363 ± 0.084	0.697 ± 0.370	0.114 ± 0.082	0.329 ± 0.092	0.056 ± 0.022	0.106 ± 0.066
10	0.031 ± 0.017	0.068 ± 0.019	1.875 ± 0.618	2.149 ± 0.328	1.098 ± 0.367	1.367 ± 0.217	0.485 ± 0.165	0.807 ± 0.184	0.076 ± 0.038	0.133 ± 0.079
11	0.033 ± 0.021	0.080 ± 0.027	2.415 ± 0.934	4.310 ± 0.454	2.787 ± 0.303	3.410 ± 0.535	0.722 ± 0.212	1.652 ± 0.444	0.080 ± 0.025	0.266 ± 0.113
12	0.023 ± 0.031	0.045 ± 0.019	3.982 ± 0.560	5.748 ± 0.318	4.547 ± 0.268	6.064 ± 0.286	1.494 ± 0.514	3.143 ± 0.129	0.125 ± 0.068	0.253 ± 0.081
13	0.152 ± 0.104	0.127 ± 0.072	4.548 ± 0.816	6.238 ± 0.258	4.651 ± 0.423	6.152 ± 0.242	2.107 ± 0.335	3.906 ± 0.392	0.942 ± 0.258	1.764 ± 0.219
14	0.120 ± 0.026	0.133 ± 0.057	5.829 ± 0.296	6.752 ± 0.226	4.975 ± 0.409	7.048 ± 0.520	2.227 ± 0.250	3.461 ± 0.299	1.682 ± 0.271	2.415 ± 0.337
15	0.120 ± 0.035	0.212 ± 0.058	5.587 ± 0.169	6.914 ± 0.416	5.133 ± 0.313	6.844 ± 0.223	2.057 ± 0.398	4.027 ± 0.106	2.328 ± 0.179	2.610 ± 0.133

4.1.1 Crack Density with Varying Processing Parameters

Initial observations of the micrographs suggested that solidification cracking was more prevalent at high scan speeds and low laser powers. This matches the expected relation between processing parameters and crack density, as lower energy densities increase the susceptibility of alloys to solidification cracking due to higher cooling rates. To observe the trend between processing parameters and crack density, crack density was plotted against energy density in Figure 8 for all the samples. For the Al1.5Cu samples in Figure 8a, there appears to be an inverse relationship between crack density and energy density. However, the amount of solidification cracking in the Al1.5Cu samples is very low so it is difficult to accurately observe the relationship with energy density. The small amount of cracking also results in the uncertainty being high relative to the total crack length. However, the other manufactured compositions in Figures 8b-8e have a consistent trend between crack density and energy density that appears to follow an exponential decay relation. While it appears that the trend is steeper for the Al10Cu samples compared to the other compositions that exhibit an exponential decay relationship, this is in part due to the crack density being lower and hence the y-axis is more compressed to better display the data. The consistency in the relationship between crack density and energy density across various compositions is noteworthy and supports the reliability of the crack density measurements taken. Another finding observed from Figure 8 is that the XY plane tends to exhibit a higher crack density than the XZ plane for samples of the same processing parameters and composition. This is due to the orientation of the grains being normal to the build direction, resulting in there being more grain boundaries per given area (or volume). This is a common observation in LPBF manufactured samples.

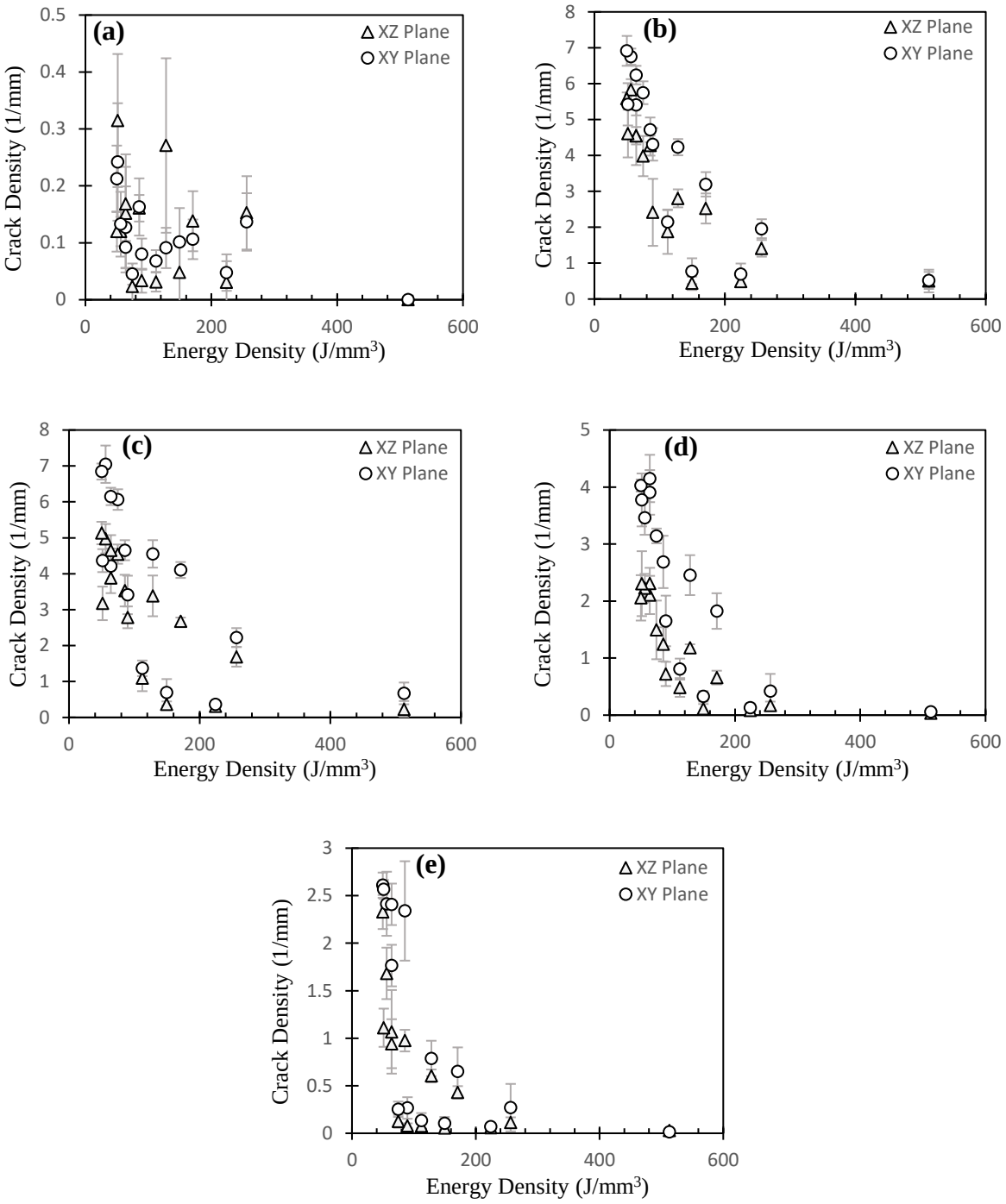

Figure 8. Plotted crack density vs energy density for binary Al-Cu samples with compositions of (a) 1.5 Wt.% Cu, (b) 3 Wt.% Cu, (c) 4.5 Wt.% Cu, (d) 6 Wt.% Cu, (e) 10 Wt.% Cu

4.1.2 Crack Density with Varying Composition

The relationship between solidification cracking and alloy composition for Al-Cu alloys manufactured through LPBF was investigated in this thesis to observe whether there is a difference compared to traditional manufacturing methods and solidification cracking models. Initial observations of the micrographs already suggested that there may be a shift in cracking susceptibility to higher solute compositions since there was far less cracking in the Al1.5Cu samples than expected from existing solidification cracking data. Figure 9 depicts the relationship between the measured crack density and alloy composition for each LPBF parameter set. A cubic spline fit was used to interpolate for the crack density at compositions between manufactured compositions. There was some minor variance in which composition corresponded to the maximum crack density, but in general, the maximum crack density occurred at a composition of approximately 3.5 wt.% Cu. This is significantly higher than 1 wt.% Cu, the composition with the maximum cracking susceptibility of Al-Cu from traditional manufacturing methods. There is a clear shift in solidification cracking susceptibility to higher solute concentrations for LPBF manufactured alloys. Some additional observations from Figure 9 that match previous findings are that crack density increases with scan speed and that the XY plane had more cracking than the XZ plane. This is due to a decrease in energy density and grain orientation respectively, as previously explained. Also, while there is more cracking in the samples manufactured at 350W (Figures 9a and 9b) compared to 200W (Figures 9c and 9d), this is due to lower scan speeds being used with the 200W samples. For samples manufactured at the same scan speed, it would be expected that the 200W samples would have more cracking since the energy density would be lower.

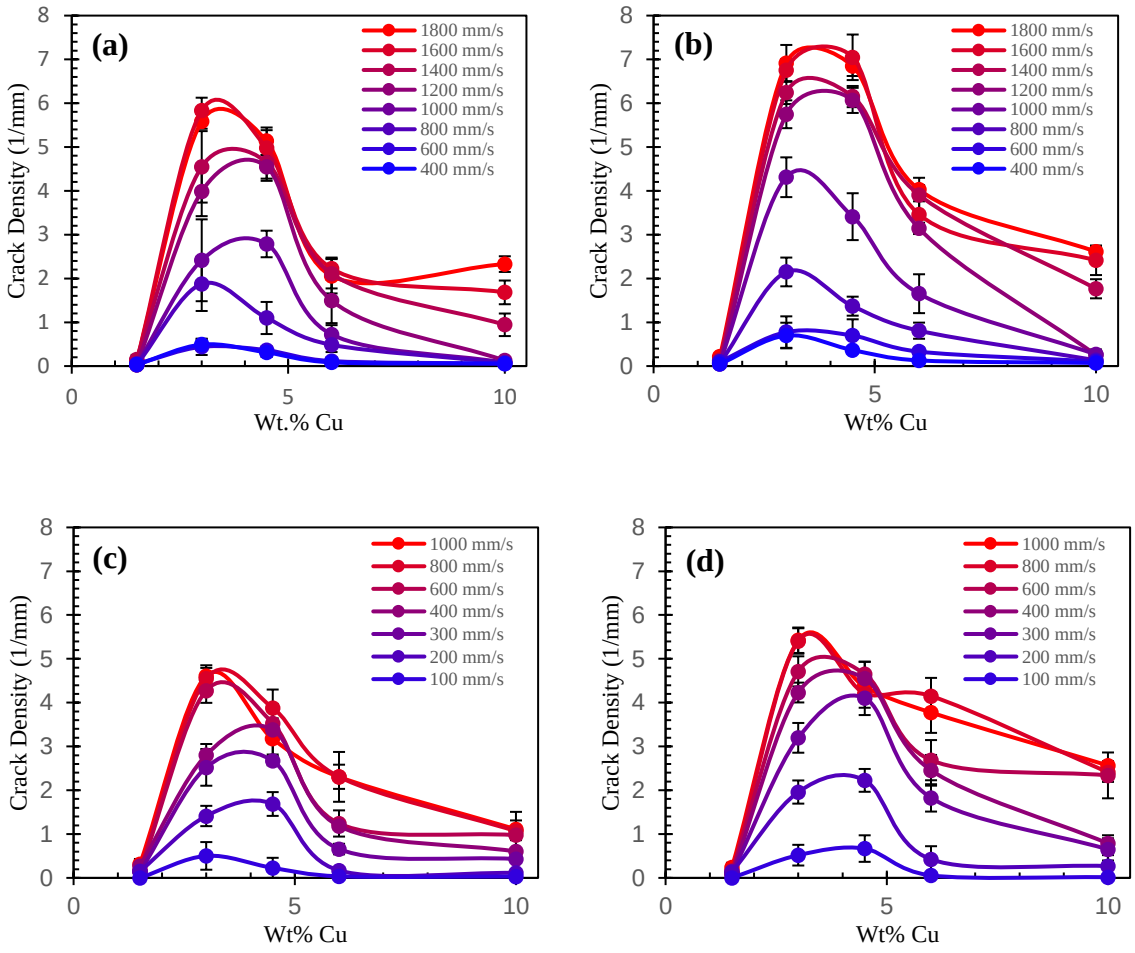

Figure 9. Plotted crack density vs composition at constant processing parameters for the manufactured Al-Cu samples. For clarity and ease of comparison, the graphs were organized by laser power and cross-section, with various scan speeds being displayed within the plot. (a) 350W / XZ plane, (b) 350W / XY plane, (c) 200W / XZ plane, (d) 200W / XY plane

4.1.3 Discussion

Measurements of the crack density in Al-Cu binary alloys produced through LPBF have shown a significant shift in maximum cracking composition from ~1 wt.% Cu in traditional manufacturing methods to ~3.5 wt.% Cu. This shift in the maximum solidification cracking susceptibility towards higher solute concentrations matches the observations found by Hyer et al. [3,4] for binary Al-Si alloys manufactured through LPBF and Hu et al. [29] in his modeling of LPBF manufactured Al-Cu alloys. This discrepancy is not extensively documented, so it would be useful to analyze how traditional cracking susceptibility models for casting and welding apply to LPBF. In the following section, a modified form of the Scheil-Gulliver Equation will be used in conjunction with Kou's cracking criteria to model the cracking susceptibility of binary Al-Cu alloys. While this is a common practice that has shown success for predicting cracking in binary alloys, it has not been successfully applied to LPBF. By comparing this model to the obtained crack density data, insight can be gained into the application of the Scheil-Gulliver equation and Kou's cracking criteria to LPBF. Adjusting this existing method for modeling cracking susceptibility so that it accurately models solidification cracking for LPBF would be useful in designing alloys with a high resistance to solidification cracking. Furthermore, analyzing the discrepancies between this method of modeling solidification cracking susceptibility and the experimental results will provide insight into how the kinetics of solidification during LPBF differ from traditional manufacturing methods.

4.2 Modeling Solidification Cracking in Al-Cu Alloys

The cracking susceptibility of Al-Cu binary alloys manufactured through LPBF was modeled using a modified Scheil equation that incorporates a parameter for back-diffusion during solidification, in conjunction with Kou's cracking criteria. The modified Scheil-Gulliver equation was utilized to find the relationship between T and f_s for various compositions so that Kou's cracking criteria, which defines the solidification cracking susceptibility index as the maximum value of $\left|dT/df_s^{1/2}\right|$ near complete solidification of the alloy, can be used to find cracking susceptibility in relation to alloy composition. Equation (11), which is derived from the modified Scheil-Gulliver equation developed by Kurz and Fisher [26], was used to incorporate the effect of back-diffusion into solidification cracking behavior. This was used instead of the unmodified Scheil equation since the work of Hyer et al. [3,4] suggested that solid-state diffusion during solidification may be more significant in LPBF manufacturing, despite this manufacturing method having high cooling rates. All constants in Equation (11) were taken directly from the equilibrium phase diagram for Al-Cu except Ω. While k is dependent on alloy composition, k was taken as a constant independent of composition by approximating the solidus and liquidus as straight lines. k was calculated using Equation (6), in which C_S is the solute solubility in the solid phase, and C_L is the solute solubility in the liquid phase. Since linear liquidus and solidus lines are being taken as an approximation, k can be calculated by taking C_S to be the solubility of Cu in Al at the eutectic temperature (5.65 Wt.% Cu) and C_L as the eutectic composition (32.7 Wt.% Cu). Hence from the equilibrium phase diagram for Al-Cu, T_f was taken as 660.452 °C, k was calculated as 0.173, and T_L was dependent on composition. The value of T_L at various compositions was found by using solidification simulations in Thermo-Calc under equilibrium conditions.

The only remaining constant that needed to be approximated was Ω, which is a constant derived from α, the back-diffusion Fourier number, and defined by Equation (8). α is dependent on processing parameters and composition, but for the sake of simplicity, it is typically taken as a constant when used in the modified Scheil equation. Equation (7) allowed for the calculation of α from the solid-state diffusion coefficient D_S, the freezing time t_f, and the characteristic length L. D_S can vary somewhat with composition, but was approximated as a composition-independent constant so that α could remain an invariable constant in the Scheil equation. L is taken as half of the secondary dendrite arm spacing (SDAS), which is highly cooling rate dependent and hence dependent on processing parameters. Likewise, t_f is also dependent on the cooling rate.

To approximate α, Equation (7) was simplified. First, by taking the characteristic length as half of the SDAS, Equation (7) was rewritten as Equation (12) with λ being the SDAS.

$$\alpha = \frac{4D_S t_f}{\lambda^2} \tag{12}$$

Both t_f and λ are dependent on the cooling rate, so this equation was simplified further. t_f is defined as the ratio of the freezing range to the cooling rate, and hence can be expressed by Equation (13) in which ΔT and $\dot{T}$ are the freezing range and cooling rate, respectively. λ can be related to the cooling rate through Equation (14) [35], which is a common approximation used for LPBF alloys. Note that in Equation (14), the units for the SDAS must be in micrometers for this relationship to be accurate for the given constants. In Equation 14, A and n are material constants that are composition-dependent, but since the goal was to develop a simple approximation for λ, A and n were taken as constants for Al5Cu as 42 and 0.33 respectively [36]. Substituting Equations

(13) and (14) for the freezing time and SDAS into Equation (12) for α simplified into Equation (15).

$$t_f = \frac{\Delta T}{\dot{T}} \tag{13}$$

$$\lambda = A\dot{T}^{-n} \tag{14}$$

$$\alpha = \frac{4D_S\Delta T}{A^2\dot{T}^{-2n+1}} \tag{15}$$

D_S is a temperature-dependent constant that was calculated using Equation (16), the Arrhenius equation. In this equation, D_0 and Q are material constants that were taken from literature as 6.5×10^{-5} m^2/s and 136,000 J/mol, respectively [37]. D_S was calculated at 600°C, as this is an intermediate value within the range of solidification temperatures experienced by Al-Cu alloys, which gave a calculated value of 4.255×10^{-13} m^2/s. Experimental results for the value of D_S at temperatures near the melting temperature for Al-Cu alloys are typically on the order of 10^{-13}, so this appears to be a reasonable approximation.

$$D_S = D_0 e^{-Q/RT} \tag{16}$$

The freezing range (ΔT) is defined as the temperature range over which solidification occurs, and hence is a composition-dependent term taken from the equilibrium phase diagram. Ṫ can be approximated using a variation of the Rosenthal equation [35] developed for LPBF processing in which scan speed and laser power impact the calculation of the cooling rate. This adaptation of the Rosenthal equation is expressed in Equation (17), in which κ is the thermal conductivity of the liquid, T_S is the solidus temperature, T_L is the liquidus temperature, T_0 is the

temperature of the build plate, v is the scan speed, and Q is the absorbed laser power. Q can be taken as the laser power multiplied by the absorptivity of the alloy. κ was taken from literature to be 90 W/m*K [38] and the absorptivity was approximated as 0.2 [39]. The build plate was kept at a constant 100 ℃ during the LPBF process so T_0 is 100 ℃. T_S and T_L are composition-dependent and were obtained from the equilibrium phase diagram. Since $\dot{T}$ can vary by multiple orders of magnitude depending on composition and processing parameters, it is difficult to give an approximate value that is not composition dependent. Likewise, ΔT is highly dependent on composition, so a general approximation is difficult to ascertain. Instead, the cooling rate and freezing range were calculated for each composition, so that a value for α could be calculated for each manufactured sample.

$$\dot{T} = 2\pi\kappa(T_S - T_0)(T_L - T_0)\frac{v}{Q} \tag{17}$$

Table 4 lists all calculated cooling rates and α approximated using Equations (15) and (17) for all compositions and processing parameters. For the processing parameters and compositions of the manufactured samples, the cooling rate varied from 3.91×10^5 to 4.29×10^6 K/s with an average value of 2.23×10^6 K/s. The value of α varied from 1.38×10^{-4} to 6.24×10^{-4} with an average value of 3.40×10^{-4}. Henceforth, 3.4×10^{-4} will be taken as an approximation for the "literature value" of α. This is a very small value for α, implying that back-diffusion would be insignificant during solidification.

Table 4. Approximations of cooling rate and α for all manufactured samples

		1.5 Wt.% Cu		*3 Wt.% Cu*		*4.5 Wt.% Cu*		*6 Wt.% Cu*		*10 Wt.% Cu*	
		Cooling Rate (K/s)	**α**	**Cooling Rate (K/s)**	**α**	**Cooling Rate (K/s)**	**α**	**Cooling Rate (K/s)**	**α**	**Cooling Rate (K/s)**	**α**
Energy Density (J/mm^3)	49.9	4.29E+06	1.38E-04	4.02E+06	2.83E-04	4.02E+06	2.83E-04	4.02E+06	2.83E-04	4.02E+06	2.83E-04
	51.3	4.17E+06	1.39E-04	3.91E+06	2.85E-04	3.91E+06	2.85E-04	3.91E+06	2.85E-04	3.91E+06	2.85E-04
	56.1	3.82E+06	1.44E-04	3.58E+06	2.94E-04	3.58E+06	2.94E-04	3.58E+06	2.94E-04	3.58E+06	2.94E-04
	64.1	3.34E+06	1.50E-04	3.13E+06	3.08E-04	3.13E+06	3.08E-04	3.13E+06	3.08E-04	3.13E+06	3.08E-04
	64.1	3.34E+06	1.50E-04	3.13E+06	3.08E-04	3.13E+06	3.08E-04	3.13E+06	3.08E-04	3.13E+06	3.08E-04
	74.8	2.86E+06	1.58E-04	2.68E+06	3.24E-04	2.68E+06	3.24E-04	2.68E+06	3.24E-04	2.68E+06	3.24E-04
	85.5	2.50E+06	1.66E-04	2.35E+06	3.39E-04	2.35E+06	3.39E-04	2.35E+06	3.39E-04	2.35E+06	3.39E-04
	89.7	2.39E+06	1.68E-04	2.24E+06	3.45E-04	2.24E+06	3.45E-04	2.24E+06	3.45E-04	2.24E+06	3.45E-04
	112.2	1.91E+06	1.82E-04	1.79E+06	3.72E-04	1.79E+06	3.72E-04	1.79E+06	3.72E-04	1.79E+06	3.72E-04
	128.2	1.67E+06	1.90E-04	1.56E+06	3.90E-04	1.56E+06	3.90E-04	1.56E+06	3.90E-04	1.56E+06	3.90E-04
	149.6	1.43E+06	2.00E-04	1.34E+06	4.11E-04	1.34E+06	4.11E-04	1.34E+06	4.11E-04	1.34E+06	4.11E-04
	170.9	1.25E+06	2.10E-04	1.17E+06	4.30E-04	1.17E+06	4.30E-04	1.17E+06	4.30E-04	1.17E+06	4.30E-04
	224.4	9.54E+05	2.30E-04	8.94E+05	4.71E-04	8.94E+05	4.71E-04	8.94E+05	4.71E-04	8.94E+05	4.71E-04
	256.4	8.35E+05	2.41E-04	7.82E+05	4.93E-04	7.82E+05	4.93E-04	7.82E+05	4.93E-04	7.82E+05	4.93E-04
	512.8	4.17E+05	3.05E-04	3.91E+05	6.24E-04	3.91E+05	6.24E-04	3.91E+05	6.24E-04	3.91E+05	6.24E-04

4.2.1 Modeling Solidification Cracking for Equilibrium Values of α and k

With the literature value of α being approximated as 3.40×10^{-4} and all other constants in the modified Scheil equation being obtainable from the equilibrium phase diagram, plots were made to relate T and $f_s^{1/2}$ for varying alloy compositions. Since α is approximated as a constant independent of composition, the only parameter within the modified Scheil equation that varies with composition is the liquidus temperature, T_L. Kou's cracking criteria defines cracking susceptibility in terms of the slope of the $f_s^{1/2}$ vs T curve, so Equation (11) was modified to give the relationship of $f_s^{1/2}$ and T.

From Equation (11), plots of $f_s^{1/2}$ vs T were obtained for compositions from pure Al to Al10Cu in increments of 0.5 wt.% Cu as presented in Figure 10. These plots were developed using an iterative process in which T was varied between the melting temperature of Al (660.452°C) and the eutectic temperature (548.2°C), and the corresponding values of f_s were calculated using equation 11. A cubic spline was used between the data points to produce a smooth curve. As the concentration of solute increases, the curve shifts down and to the left. This means that for compositions with more Cu, solidification begins at a lower temperature and has a lower f_s by the time the eutectic temperature is reached. Without considering the upper bound of f_s at which solidification cracking will no longer occur, lower concentrations of solute have the largest slopes and would be considered the most susceptible to cracking. This is not the case in existing experimental findings, which demonstrates the need to set an appropriate upper bound on f_s when solving for Kou's cracking criteria.

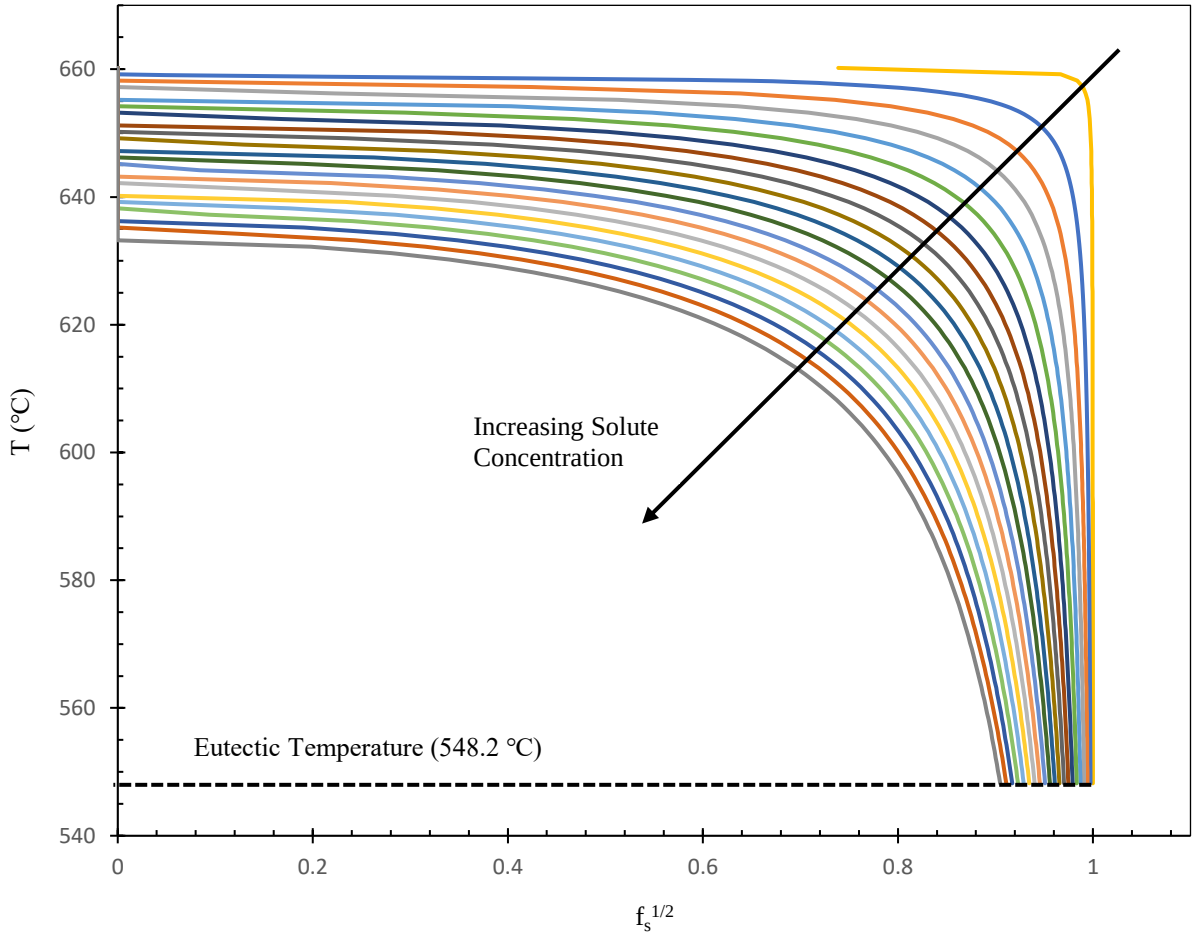

Figure 10. Plotted $fs^{1/2}$ vs T for various compositions of Al-Cu binary alloys. Compositions vary from pure Al to Al10Cu in increments of 0.5 wt.% Cu.

The solidification cracking susceptibility index was defined as the maximum value of $\left|dT/df_s^{1/2}\right|$ near complete solidification. "Near complete solidification" is defined as the solidification range over which grain separation and solidification cracking occurs, which can be considered as the fraction solidified of the mushy zone. The lower bound is somewhat arbitrary in its importance for calculating the cracking susceptibility index since the maximum value of $\left|dT/df_s^{1/2}\right|$ will increase with f_s. The upper bound, however, greatly impacts the resulting

cracking susceptibility curve. Since other studies have had success in modeling solidification cracking for casting and welding applications using the range of $0.9 > f_s > 0.99$ [2], the same f_s range will be used for this analysis with a slightly smaller lower bound. This lower bound was adjusted since later calculations of Kou's cracking criteria had compositions that did not reach 0.9 by the time the eutectic temperature was reached, so it would be necessary to change the lower bound to get meaningful results. The maximum value of $\left|dT/df_s^{1/2}\right|$ was calculated from Figure 10 for $0.8 < f_s < 0.99$ at each composition and taken as the cracking susceptibility index. The resulting graph of composition vs cracking susceptibility index is displayed in Figure 11. Interestingly, the maximum value of the cracking susceptibility index is at the same composition that has been experimentally observed to have the most cracking for traditional manufacturing methods. Based on Figure 11, there must be a discrepancy in either the modified Scheil equation or Kou's cracking criteria that prevents this method from accurately modeling solidification cracking for LPBF, despite its success in casting and welding applications.

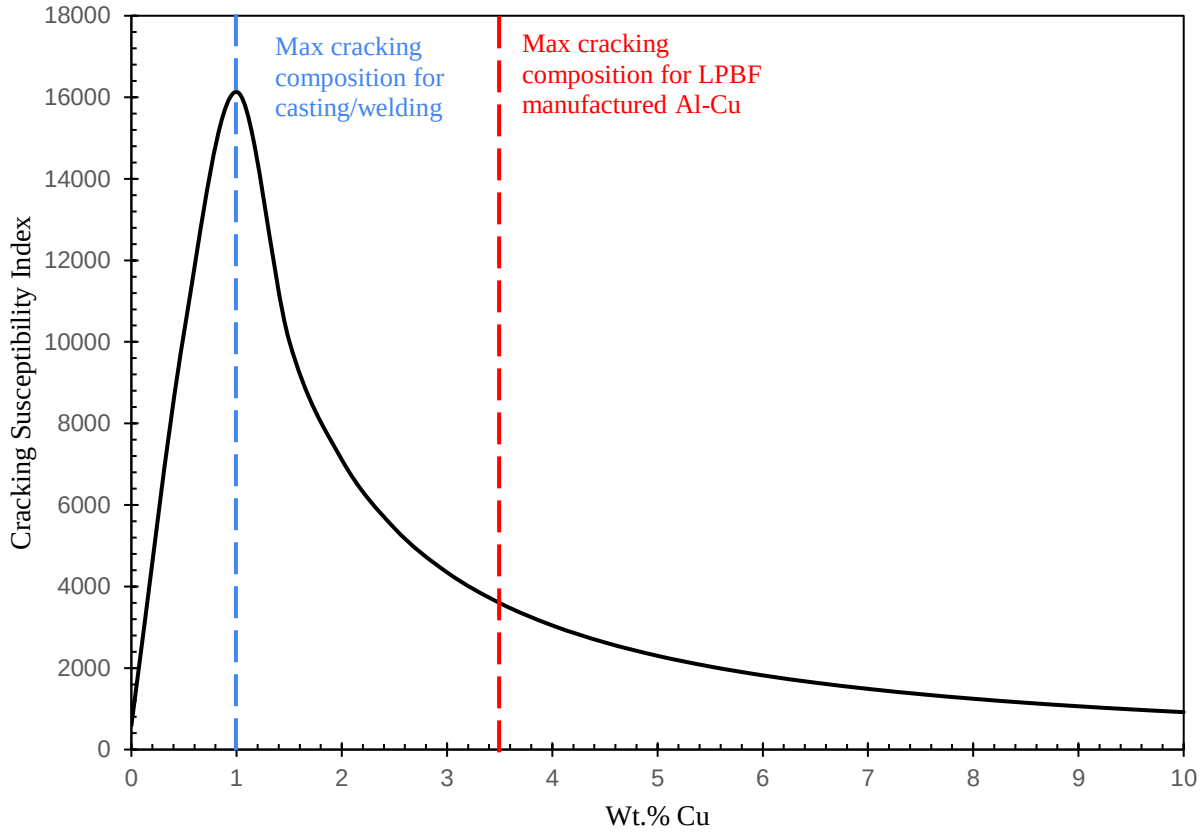

Figure 11. Plot of composition vs cracking susceptibility index using the literature value for α and the equilibrium value of the partition coefficient ($3.40*10^{-4}$ and 0.173 respectively). The blue line shows the composition of Al-Cu alloys with the most cracking in traditional manufacturing methods, while the red line shows the composition with the most cracking for LPBF.

Mathematically, increasing the value of α or k will cause a shift in the maximum cracking susceptibility to a higher solute concentration. α may be higher than its literature value due to the solid-state diffusion coefficient being higher than anticipated. Typically, the Arrhenius equation is used to model D_S for a solid based on the atom-vacancy exchange mechanism. During LPBF, the solidified component during solidification is surrounded by a liquid phase with a higher diffusion coefficient, so there may be mechanisms of diffusion other than simple atom-vacancy exchange. Another possibility is that the partition coefficient may be higher than equilibrium due to the very

high cooling rates associated with LPBF. In LPBF, the cooling rates are high enough that rapid solidification occurs, resulting in solute trapping and reduced partitioning [5]. This causes the partition coefficient to increase and approach unity as the composition of the liquid and solid states become more similar. Since both explanations are viable possibilities as to why there is a shift in maximum cracking composition to higher solute concentrations, investigating the values of these coefficients that would match the measured crack density data will provide insight into solidification cracking for LPBF.

4.2.2 Examining the Feasibility of Increasing D_S and k

To test the feasibility of increased solid-state diffusion shifting the maximum cracking susceptibility, k was left at its equilibrium value, and the value of α was found that corresponds to a maximum cracking susceptibility index at Al3.5Cu. Using an iterative equation solver, α was taken as a variable, k was taken as a constant at its equilibrium value of 0.173, and the cracking susceptibility index was calculated for Al-Cu alloys with compositions of 0 to 10 wt.% Cu in increments of 0.5 Wt.%. The conditions placed on the equation solver were that the maximum value of the cracking susceptibility index occurred at Al3.5Cu and that the difference in cracking susceptibility index between Al3Cu and Al4Cu was minimized. This will ensure that the maximum cracking susceptibility index will lie at a composition as close to Al3.5Cu as possible. With these conditions, the value of α was determined as 0.175. Figure 12 shows the cracking susceptibility plot developed using this increased value of α and the equilibrium value of the partition coefficient. The peak of the cracking susceptibility index matches the experimental data, and the magnitude of the cracking susceptibility index has been significantly reduced.

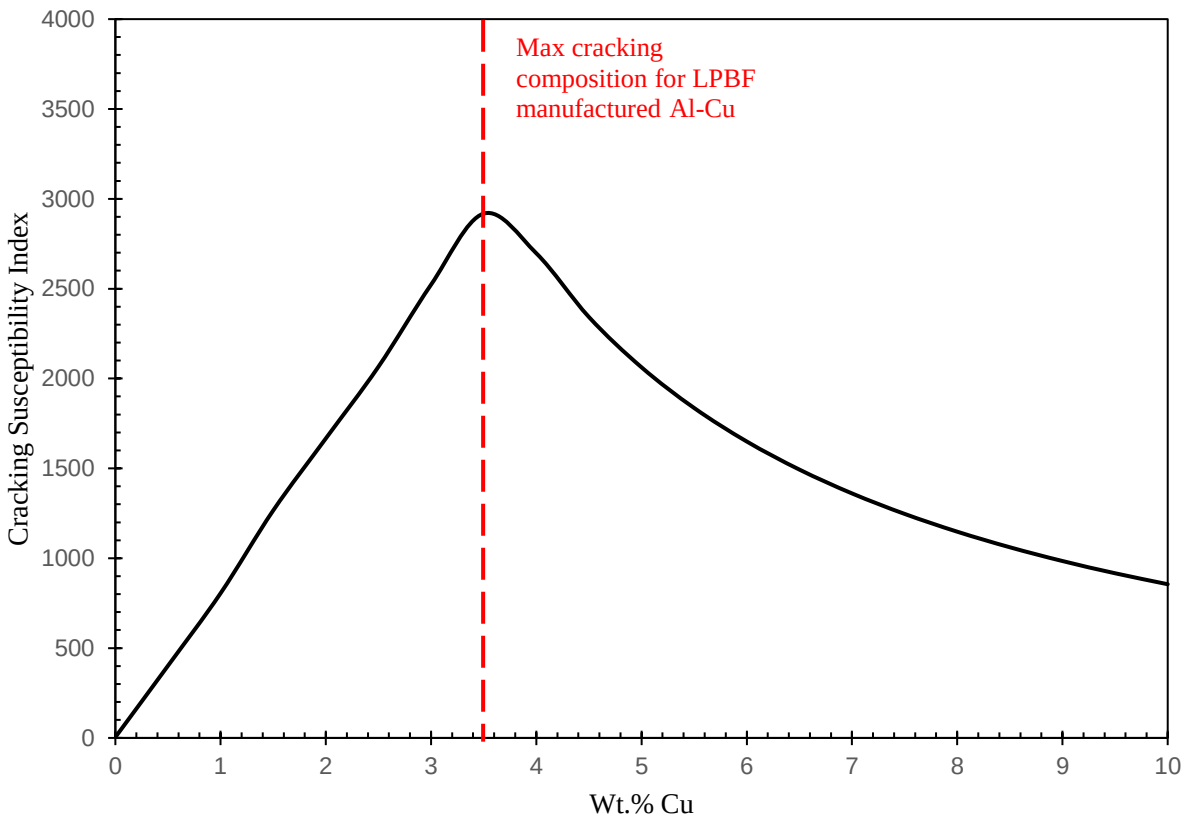

Figure 12. Plot of composition vs cracking susceptibility index using $\alpha = 0.175$ and the equilibrium value of the partition coefficient ($k = 0.173$)

To analyze whether a value of 0.175 is feasible for α, the solid-state diffusion coefficient that would correspond to this value of α was calculated. Equation (15) can be re-written to solve for D_S in terms of α as Equation (18). In this equation, the cooling rate and freezing range are largely dependent on processing parameters and alloy compositions, so rather than approximating these constants, D_S was calculated for the processing parameters and compositions of all manufactured samples. The calculated values of D_S are compiled in Table 5. The value for D_S varied from 6.40×10^{-11} to 5.40×10^{-10} m^2/s with an average value of 2.02×10^{-10} m^2/s. The literature value for D_S near solidification temperatures was found to be 4.255×10^{-13} m^2/s while

the diffusion coefficient for the liquid state is typically on the order of 10^{-8} near solidification temperatures. Since the calculated value for D_S falls in the middle of these values, α being as high as 0.175 may be possible.

$$D_S = \frac{\alpha A^2 \dot{T}^{-2n+1}}{4\Delta T} \tag{18}$$

Table 5. Calculation of D_S for all manufactured samples when $\alpha = 0.175$

		1.5wt%		3wt%		4.5wt%		6wt%		10wt%	
		Cooling Rate (K/s)	**Ds (m^2/s)**	**Cooling Rate (K/s)**	**Ds (m^2/s)**	**Cooling Rate (K/s)**	**Ds (m^2/s)**	**Cooling Rate (K/s)**	**Ds (m^2/s)**	**Cooling Rate (K/s)**	**Ds (m^2/s)**
Energy Density (J/mm3)	49.9	4.29E+06	5.40E-10	4.02E+06	2.63E-10	4.02E+06	1.76E-10	4.02E+06	1.41E-10	4.02E+06	1.60E-10
	51.3	4.17E+06	5.35E-10	3.91E+06	2.61E-10	3.91E+06	1.74E-10	3.91E+06	1.40E-10	3.91E+06	1.58E-10
	56.1	3.82E+06	5.19E-10	3.58E+06	2.53E-10	3.58E+06	1.69E-10	3.58E+06	1.36E-10	3.58E+06	1.54E-10
	64.1	3.34E+06	4.96E-10	3.13E+06	2.42E-10	3.13E+06	1.61E-10	3.13E+06	1.30E-10	3.13E+06	1.47E-10
	64.1	3.34E+06	4.96E-10	3.13E+06	2.42E-10	3.13E+06	1.61E-10	3.13E+06	1.30E-10	3.13E+06	1.47E-10
	74.8	2.86E+06	4.70E-10	2.68E+06	2.30E-10	2.68E+06	1.53E-10	2.68E+06	1.23E-10	2.68E+06	1.39E-10
	85.5	2.50E+06	5.40E-10	2.35E+06	2.19E-10	2.35E+06	1.46E-10	2.35E+06	1.18E-10	2.35E+06	1.33E-10
	89.7	2.39E+06	4.42E-10	2.24E+06	2.16E-10	2.24E+06	1.44E-10	2.24E+06	1.16E-10	2.24E+06	1.31E-10
	112.2	1.91E+06	4.10E-10	1.79E+06	2.00E-10	1.79E+06	1.33E-10	1.79E+06	1.07E-10	1.79E+06	1.21E-10
	128.2	1.67E+06	3.92E-10	1.56E+06	1.91E-10	1.56E+06	1.27E-10	1.56E+06	1.03E-10	1.56E+06	1.16E-10
	149.6	1.43E+06	3.72E-10	1.34E+06	1.81E-10	1.34E+06	1.21E-10	1.34E+06	9.73E-11	1.34E+06	1.10E-10
	170.9	1.25E+06	3.55E-10	1.17E+06	1.73E-10	1.17E+06	1.16E-10	1.17E+06	9.30E-11	1.17E+06	1.05E-10
	224.4	9.54E+05	3.24E-10	8.94E+05	1.58E-10	8.94E+05	1.05E-10	8.94E+05	8.48E-11	8.94E+05	9.59E-11
	256.4	8.35E+05	3.09E-10	7.82E+05	1.51E-10	7.82E+05	1.01E-10	7.82E+05	8.10E-11	7.82E+05	9.17E-11
	512.8	4.17E+05	2.44E-10	3.91E+05	1.19E-10	3.91E+05	7.95E-11	3.91E+05	6.40E-11	3.91E+05	7.24E-11

The feasibility of the partition coefficient being higher than its equilibrium value was also examined by determining the value of k required to match the experimental findings when α is taken at its literature value. Using the same equation solver, α was taken as a constant at its literature value of 3.4×10^{-4} and k was variable. Using the same conditions of there being a maximum cracking susceptibility at Al3.5Cu and a minimum difference in cracking susceptibility index between Al3Cu and Al4Cu, the partition coefficient was found to be 0.46. Figure 13 shows the cracking susceptibility plot for k = 0.46 and $\alpha = 3.4 \times 10^{-4}$. The peak cracking susceptibility index matches the experimental data, but the magnitude of the cracking susceptibility index has not been reduced to the same extent as when α was varied instead of k.

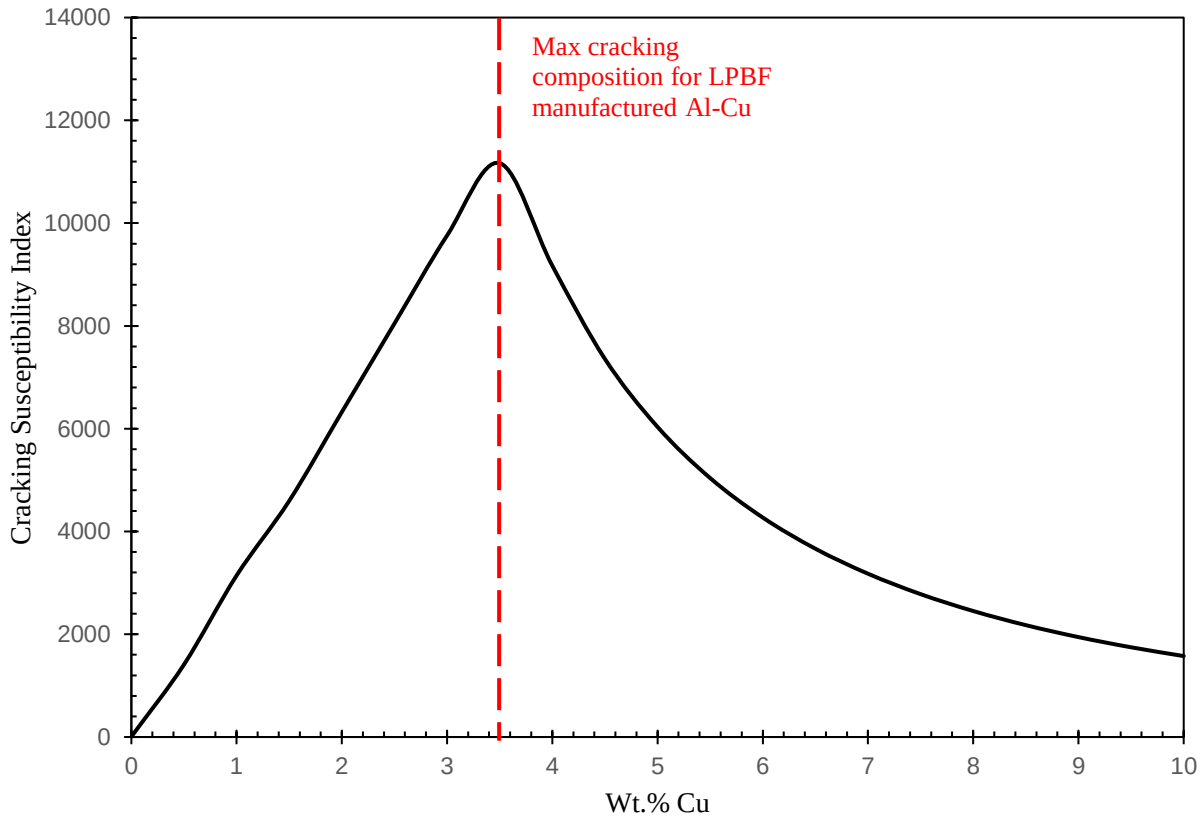

Figure 13. Plot of composition vs cracking susceptibility index using k = 0.46 and the literature value of the back-diffusion Fourier number ($\alpha = 3.4 \times 10^{-4}$)

Based on existing literature, a partition coefficient of 0.46 seems reasonable for LPBF manufactured Al-Cu alloys. Rapid solidification during LPBF has been observed experimentally for Al-alloys, with Qin [30] finding evidence of solute trapping in the microstructure of AlSi10Mg alloys, and Ghoncheh [31] measuring a partition coefficient larger than its equilibrium value in an A205 alloy. While there is not ample research in quantifying the partition coefficient for LPBF Al-Cu hypoeutectic alloys, Smith and Aziz [40] measured the partition coefficient in Al-0.15Cu during pulsed laser melting, which has comparable cooling rates to LPBF. By matching experimental findings of the solute's concentration profile to diffusion simulations, values of k were approximated for different solid-liquid interface velocities. It was found that k ~ 0.205 when the interface velocity was 0.6, and interface velocities of 1.8 and higher showed a strong deviation from the equilibrium partition coefficient, with k increasing exponentially. Since this interface velocity was achieved with comparable cooling rates to LPBF, it is reasonable that k may be significantly higher than its equilibrium value.

To better display the effectiveness of increasing α and k to match the experimental data, Figures 11, 12, 13, were normalized and compared to the experimentally results in Figure 14. In Figure 14, Figures 11, 12, and 13 are labeled as "Equilibrium Conditions", "α = 0.175", and "k = 0.46", respectively. The experimental crack density was measured with respect to composition in the XY and XZ planes at various processing parameters, so a representative data set was used for the experimental data to make a simple comparison to the developed models. The experimental data used was the crack density in the XZ plane of the samples manufactured at 1400 mm/s and 350W.

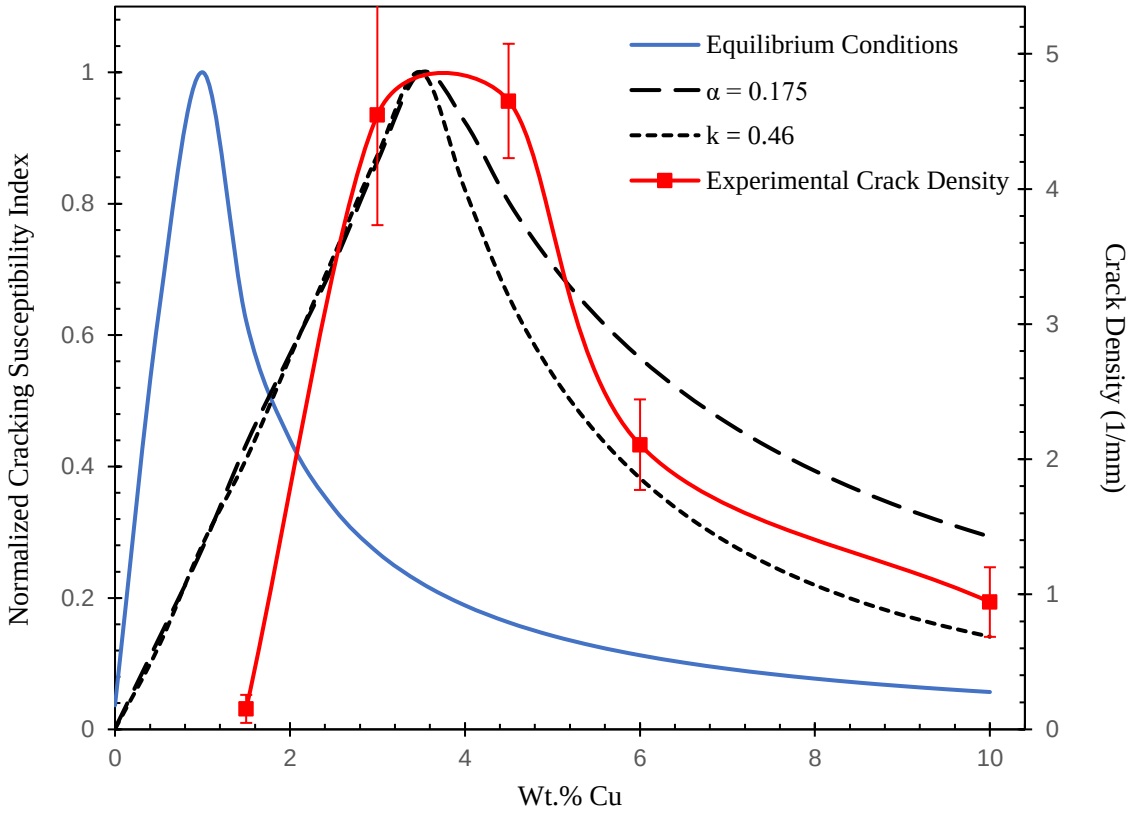

Figure 14. Comparison of the experimental data to the Figures 11-13. Figures 11-13 have been normalized on the primary y-axis, while the experimental crack density utilizes the secondary axis.

From Figure 14, increasing α to 0.175 or increasing k to 0.46 results in a cracking susceptibility curve that closely resembles the experimentally measured relationship between crack density and composition. Additionally, the cracking susceptibility curve generated using literature values of α and equilibrium values of k vary significantly from the experimental findings.

4.2.3 Parametric Study Varying α and k

For the maximum value of the cracking susceptibility index to occur at a composition near Al3.5Cu, α and/or k must be increased above their literature and equilibrium values, respectively. Increasing both α and k can be justified for LPBF applications, but it is unknown which of these is the main cause for the shift in cracking susceptibility towards higher solute concentrations. Additionally, the relative impact of increasing these parameters on the cracking susceptibility index had not been extensively documented. Therefore, a parametric study has been conducted in which α was varied from 0 to 0.3 in increments of 0.05, and k was varied at its equilibrium value of 0.173, and from 0.2 to 0.5 in increments of 0.1. The cracking susceptibility index was found relative to composition for every combination of α and k within these ranges. Using the same methodology as the cracking susceptibility graphs that have been previously generated, the modified Scheil-Gulliver equation and Kou's cracking criteria were used to find the cracking susceptibility of Al-Cu alloys with varying compositions. Compositions were varied between pure Al and Al10Cu in increments of 0.5 wt.% for every combination of α and k.

Several cracking susceptibility plots were made to display the results of the parametric study as shown in Figure 15. Each set of plots are for a constant value of α with varying values of k between the curves. As the partition coefficient increases at a constant value for α, the cracking susceptibility is reduced in magnitude and shifts towards higher solute concentrations. Also, there is significantly more cracking in the graphs at lower values of α, with the maximum cracking susceptibility index for α = 0 (Figure 15a) being ~17,000, compared to ~4,000 for α = 0.1 (Figure 15c), and ~2,300 for α = 0.2 (Figure 15e). Initial observations suggest that while increasing either parameter reduces the crack susceptibility index and increases the composition where the maximum cracking susceptibility occurs, changes in the magnitude of the cracking susceptibility

are more sensitive to α, while the shifting of the curve towards higher solute concentrations is more sensitive to k.

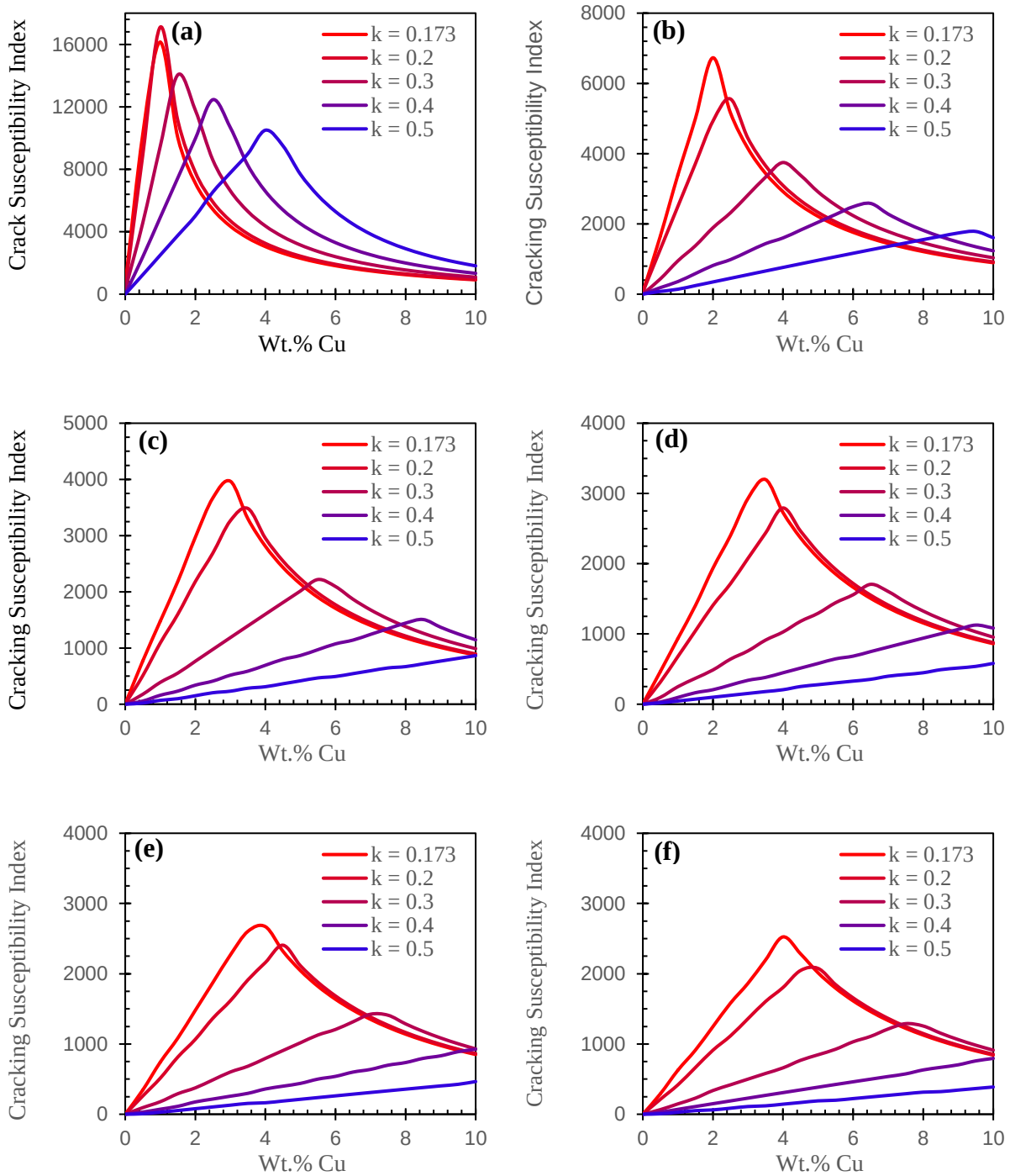

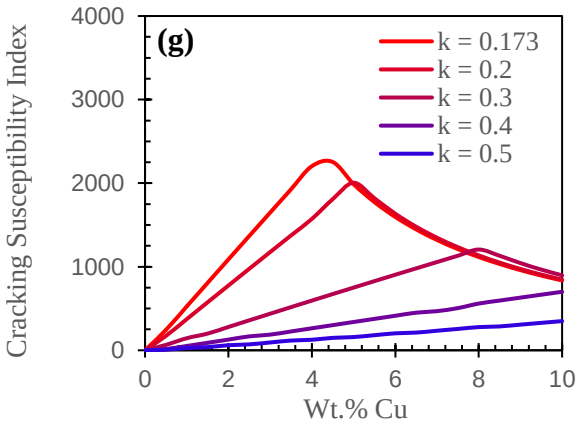

Figure 15. Plots of composition vs cracking susceptibility index varying k at a constant value for α. (a) α = 0, (b) α = 0.5, (c) α = 1, (d) α = 0.15, (e) α = 0.2, (f) α = 0.25, (g) α = 0.3

To better compare the difference between increasing α and k on the cracking susceptibility index, plots were developed to relate how increasing α and k impact the composition where the maximum value for the cracking susceptibility index occurs. Figure 16 depicts the relationship between α and the maximum cracking susceptibility composition for constant values of k. From Figure 16, it appears that increasing α has diminishing returns on shifting the cracking susceptibility curve. Furthermore, the slopes of the curves increase dramatically with increases in the partition coefficient. To better display this trend in the slope of the cracking susceptibility index, the derivative of lines of best fit from Figure 16 are plotted in Figure 17. The highest rate of change in the cracking susceptibility occurs at low values of α and high values of k, and the slope of all curves approach 0 as α increases. The first observation implies that changes in α are more effective at shifting the crack susceptibility curve at high values of k and lower values of α. The second observation supports the idea of "diminishing returns" as α increases, since the slope approaching 0 means that as α increases, the impact of changing α on the cracking susceptibility index becomes less significant. Another implication of Figure 16 is that the partition coefficient is the more

impactful parameter on shifting the composition where the maximum cracking susceptibility index occurs, since large increases of α have relatively little impact at low partition coefficients. This reaffirms the qualitative observation from Figure 15 that k appeared to be the more impactful parameter on shifting the composition of the maximum cracking susceptibility index.

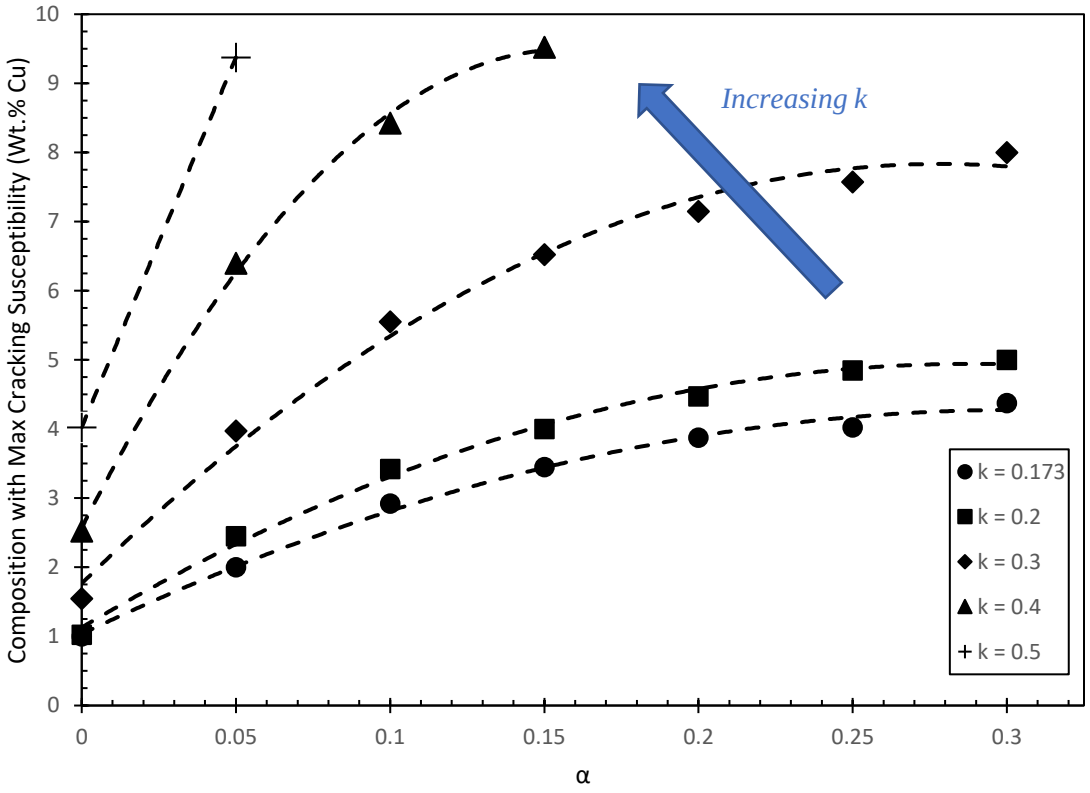

Figure 16. Plot of α vs the composition at which the maximum cracking susceptibility index occurs for constant values of k

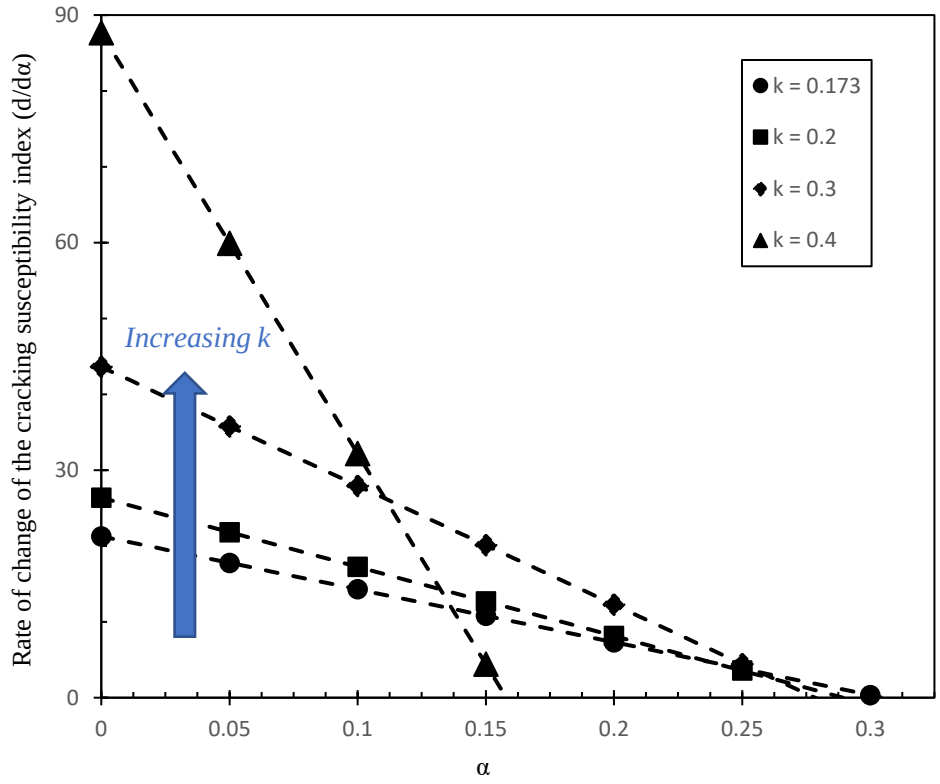

Figure 17. Plot of α vs the rate of change of the cracking susceptibility index for constant values of k

Figures 18 and 19 are similar plots to 16 and 17 respectively, but with varying values of k at constant values of α. In contrast to Figure 16 in which increasing α has diminishing returns on shifting the cracking susceptibility curves, Figure 18 shows that the cracking susceptibility curves are more sensitive to change for higher values of k. Furthermore, it can be observed in Figure 19 that the highest rate of change for the cracking susceptibility curves occurs at high values of α and high values of k, and the slope of all curves approach continually increases as k increases. This implies that if α and k are both high, small variations in the partition coefficient will greatly impact the cracking susceptibility. This is significant, as it implies that if k is large the cracking susceptibility curve is very sensitive to changes in both α and k, but if is α large the cracking

susceptibility curve is only sensitive to changes in k. Figure 19 also supports the previous observation that increasing k is more effective than α increasing at shifting the cracking susceptibility curve. Unlike in Figure 17 where α was being varied, the rate of change of the crack susceptibility curve continuously increases instead of approaching zero. While increasing α approaches a composition beyond which the maximum cracking susceptibility cannot be shifted, increasing k will continue to shift the cracking susceptibility curve at an exponential rate.

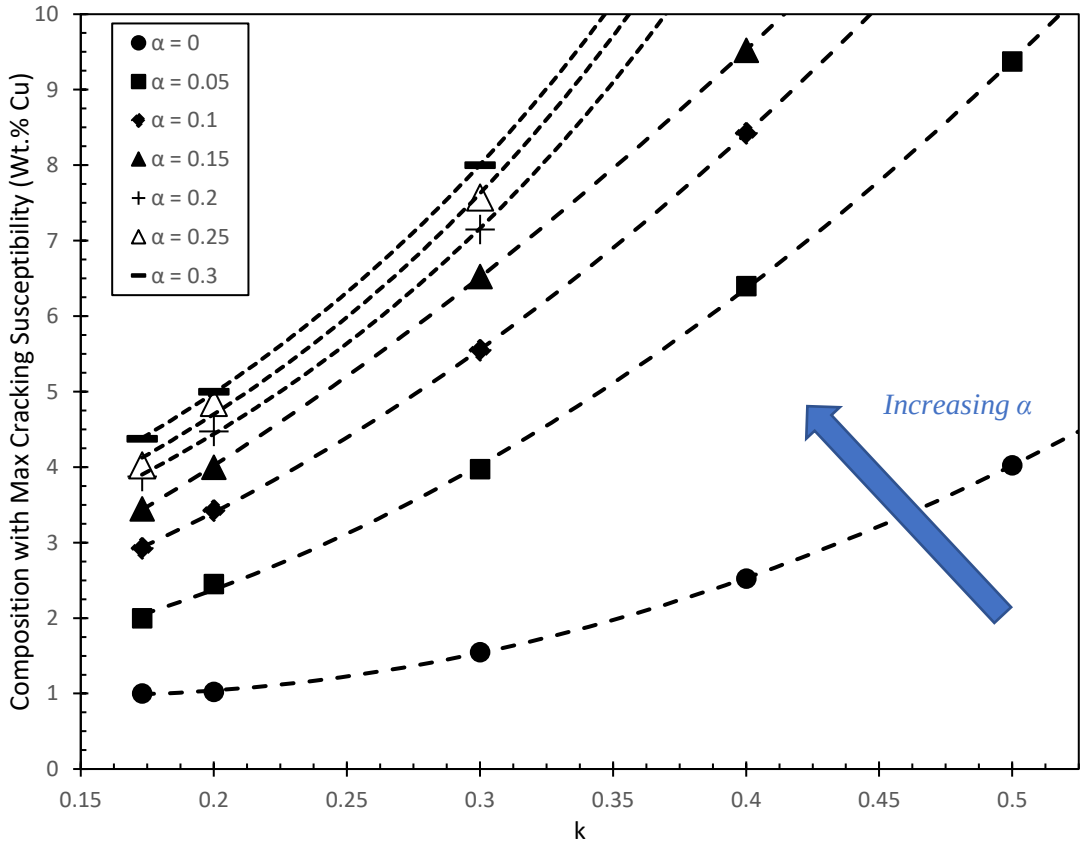

Figure 18. Plot of k vs the composition at which the maximum cracking susceptibility index occurs for constant values of α.

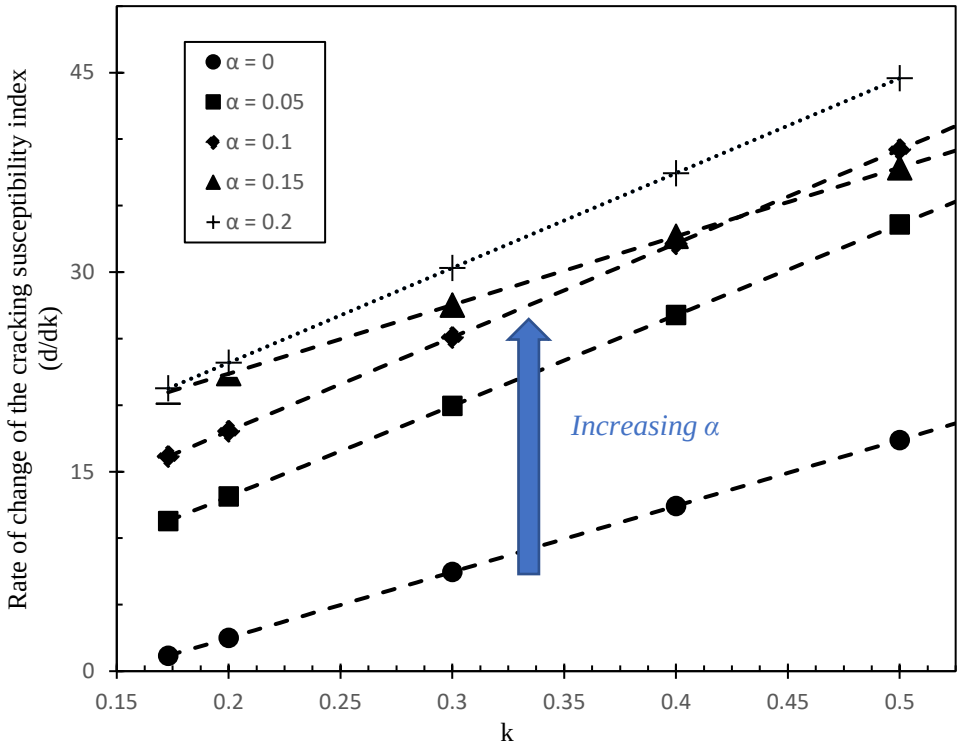

Figure 19. Plot of k vs the rate of change of the cracking susceptibility index for constant values of α

This parametric study on how α and k impact the composition at which the maximum cracking susceptibility index occurs can be summarized using the contour plot in Figure 20. From Figure 20, the cracking susceptibility curve is more sensitive to changes in α when α is low and k is high, re-affirming the results from Figures 16 and 17. Additionally, for the maximum cracking susceptibility index to shift to compositions above 12 wt.% Cu, k is required to be very large while there is not as strict of a requirement on α. This implies that k is the more important factor for shifting the cracking susceptibility index, which was also a conclusion drawn from Figures 16 through 19. The experimental data falls in the middle of the 2 to 4.5 wt.% Cu range, so this plot gives a general idea for what values of α and k are possible to match the experimental data.

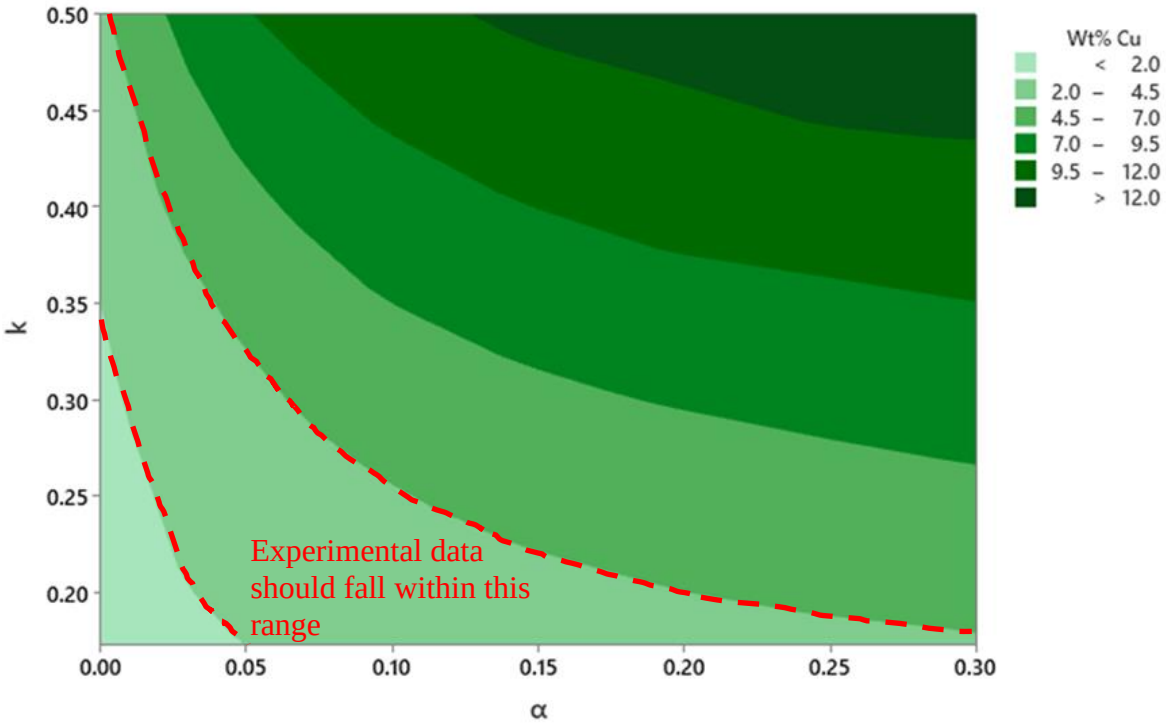

Figure 20. Contour plot of how α and k impact the composition where the maximum cracking susceptibility index occurs

4.2.4 Relation Between α and k

Since the composition at which the maximum cracking susceptibility index occurs can be calculated from α and k, and the experimental results suggest that the maximum cracking susceptibility should occur at approximately 3.5 Wt.% Cu, a relationship can be developed between α and k that would be helpful to match the experimental results. Previously, an equation solver was used to find the value of α required to match the experimental results when k was kept at its equilibrium value. Using the same methodology, k was varied from 0.175 to 0.475 in increments of 0.025, and the value of α required to shift the maximum cracking susceptibility to 3.5 wt.% Cu was determined. The resulting data is plotted in Figure 21, which displays the relationship between α and k required to match the experimental findings. This relationship between α and k appeared to follow an exponential decay function, so a curve fit for exponential decay was used. The equation of the curve fit is listed as equation 19.

$$\alpha = 1.47e^{-12.47k} \tag{19}$$

This provides a direct way to calculate α for any given value of k, or k from any given α, which would give a cracking susceptibility curve that matches the experimental results. This is useful, as it cuts out the need for the extensive computation of using an equation solver. Furthermore, if an accurate literature value can be obtained for either variable in LPBF applications, it will be easy to see calculate the other variable and determine which mechanism is primarily responsible for the discrepancy between Kou's cracking criteria and the experimental results.

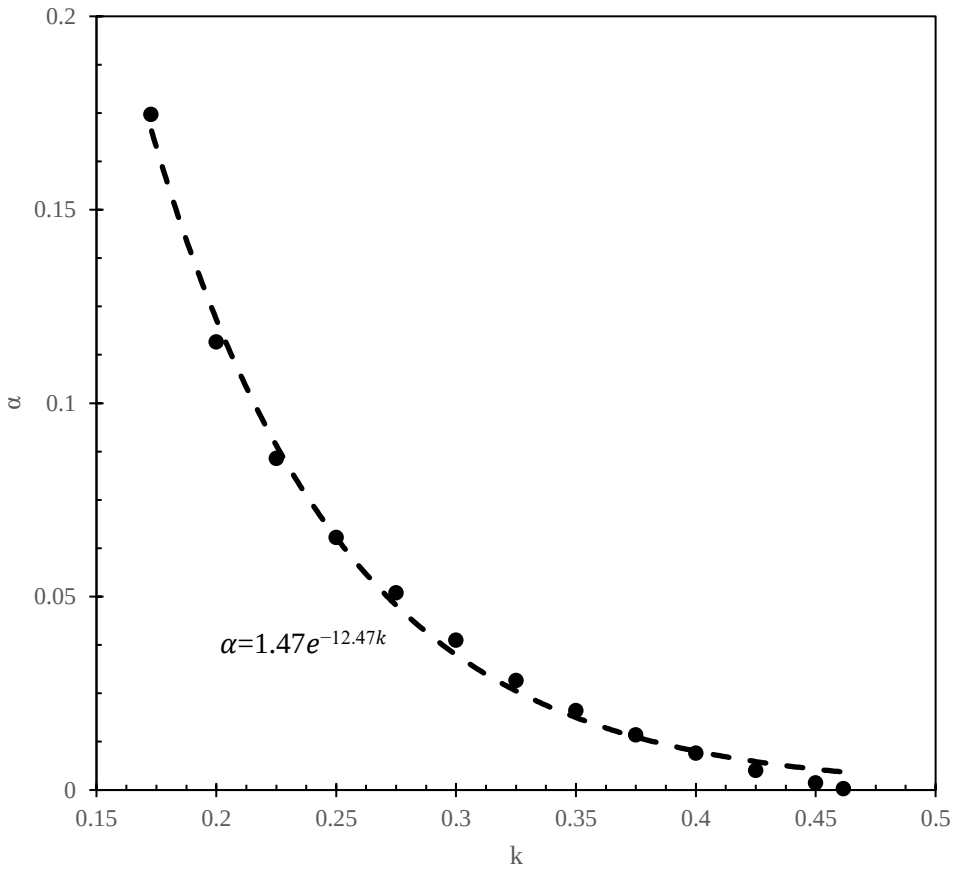

Figure 21. Plot of α vs k required for the maximum value of the cracking susceptibility index to occur at a composition of Al3.5Cu

4.2.5 Modeling the Increased Partition Coefficient

While a relationship has been developed between α and k that is required to match the experimental data, it is still unclear which variable is primarily responsible for the shift in the cracking susceptibility curve. By modeling how the partition coefficient will increase above its equilibrium value in LPBF applications, a general understanding can be developed of the extent to which α and k increase above their literature and equilibrium values, respectively. From Figure 21, the shift in the cracking susceptibility curve would be primarily due to the solute partitioning if k ~ 0.4 or higher since α will be less than 0.01. Alternatively, the shift in cracking susceptibility can be assumed to be primarily due to increased solid-state diffusion if k is near its equilibrium value of 0.173.

A common way to model the partition coefficient during rapid solidification is to use the Continuous Growth Model [41], which defines the partition coefficient as a function of the solid-liquid interface velocity. This expression is listed as Equation (20), in which v is the velocity of the liquid-solid interface, v_D is the diffusive speed, and k_e is the equilibrium partition coefficient. The diffusive speed is the velocity at which solute atoms diffuse can across the solid-liquid interface as partitioning occurs during solidification and can be considered as constant for a given alloy. Smith and Aziz [40] experimentally determined v_D for several Al-alloys and found that Al-Cu alloys have a v_D of 6.7 m/s. An Al-Cu alloy with 0.15 Wt. % Cu was used in their study since partitioning is more easily observed experimentally in alloys that have low solute concentrations, but there should be little variation in v_D at different Al-Cu alloy compositions. v_D is commonly approximated using Equation (21) [40], in which D_L is the liquid diffusivity of the solute and L is the width of the solid-liquid interface. Both variables are relatively constant for the Al-Cu alloys considered in this thesis, so v_D can reasonably be considered a composition-independent constant

at 6.7 m/s. Taking 0.173 as the equilibrium value for the partition coefficient and using 6.7 m/s for v_D, Equation (20) can be simplified for Al-Cu alloys into Equation (22) where v is expressed in m/s.

$$k = \frac{\frac{v}{v_D} + k_e}{\frac{v}{v_D} + 1} \tag{20}$$

$$v_D = \frac{D_L}{L} \tag{21}$$

$$k = \frac{v + 1.1591}{v + 6.7} \tag{22}$$

Equation (22) gives an expression for the partition coefficient of rapidly solidified Al-Cu alloys in terms of only the liquid-solid interface velocity, which is a parameter primarily dependent on cooling rate. This expression is plotted in Figure 22.

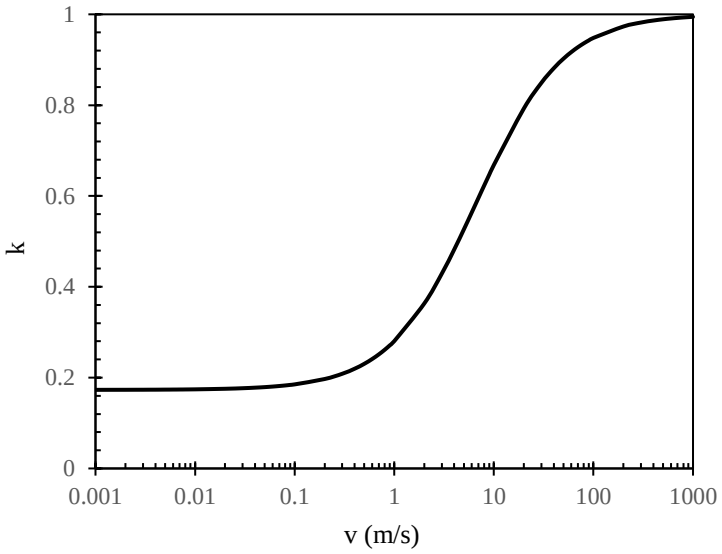

Figure 22. Plot of the partition coefficient for rapidly solidified Al-Cu alloys in terms of the solid-liquid interface velocity

For the partition coefficient to reach ~ 0.4, which would indicate that the shift in the cracking susceptibility curve is primarily due to solute trapping, a solid-liquid interface velocity of ~ 2.5 m/s would need to be achieved during solidification. Based on existing literature, this is a reasonable value to be achieved for the cooling rates associated with LPBF. McKeown et al. [42] studied the rapid solidification of an Al7Cu alloy using pulsed-laser melting, experimentally measuring the velocity of the solid-liquid interface. The interface velocity was measured by using transition electron microscopy (TEM) during the alloy's solidification to directly observe the solidification front. The cooling rates associated with pulsed-laser melting (10^5–10^7 K/s) are comparable to that of LPBF so the interface velocity should be similar as well. The maximum observed solid-liquid interface velocity was 7 m/s, which is well above what would be required to explain the shift in cracking susceptibility experimentally observed in this thesis. Since sufficiently high interface velocities have been observed under similar solidification conditions [42] and solute

trapping has been directly observed in LPBF manufactured Al-alloys [30,31], it seems as though an increase in the partition coefficient is primarily responsible for the discrepancy between Kou's cracking criteria and the experimental data.

The relationship between cooling rate and solid-liquid interface velocity in Al-Cu alloys is a potential area of further research, as it has not been experimentally determined. If the relationship between cooling rate and solidification velocity is determined, the conclusions drawn by this thesis could be more thoroughly scrutinized and the equilibrium could be defined as a function of the LPBF processing parameters through the cooling rate.

4.2.6 Discussion

The maximum crack density measured from the LPBF Al-Cu samples occurred at a higher solute concentration than predicted by the theoretical cracking susceptibility model. Two potential modifications that would shift the cracking susceptibility curve towards higher solute concentrations were presented to be feasible for LPBF manufacturing. The first possibility was that the solid-state diffusion coefficient during solidification was higher than its literature value calculated from the Arrhenius equation. This can be justified thermodynamically, as the solid phase is surrounded by liquid during solidification, which would activate the mechanism other than atom-vacancy exchange. Enhanced solid-state diffusion would increase the back-diffusion Fourier number, α, and shift the cracking susceptibility index towards higher solute concentrations. The solid-state diffusion coefficient required to account for the shift in the cracking susceptibility curve fell between the solid-state diffusion coefficient in the fully solid-state and the liquid diffusivity of Cu in Al, suggesting that this explanation is reasonable.

The second possibility was that the partition coefficient, k, was higher than its equilibrium value due to solute trapping during rapid solidification. This increase in the partition coefficient for LPBF, along with other manufacturing methods with very high cooling rates, has been well documented experimentally and would also shift the cracking susceptibility index towards higher solute compositions. While both explanations are feasible, it is important to consider which is the dominant method for shifting the cracking susceptibility curve. Between the two possible mechanisms, it seems that the partition coefficient being higher due to rapid solidification is better justified by existing literature. Not only has solute trapping been observed in LPBF manufactured Al-alloys [30,31], but solid-liquid interface velocities that are more than high enough to account for the shift in cracking susceptibility have been observed in the pulsed-laser melting of

hypoeutectic Al-Cu [42]. Additionally, in Kou's original study that defined the cracking susceptibility index [2], the unmodified Scheil-Gulliver equation was used to find the relationship between T and $f_s^{1/2}$. The predicted composition with the highest susceptibility to solidification cracking matched the experimentally observed cracking susceptibility of Al-Cu in casting or welding. If the primary discrepancy between the cracking susceptibility model and the experimental data in LPBF applications was due to there being more solid-state diffusion than anticipated from literature values, then one would expect that Kou's application of the unmodified Scheil-Gulliver equation would have the same discrepancy for casting or welding. This is especially true since the cooling rate for casting or welding is many orders of magnitude lower than that of LPBF, suggesting that solid-state diffusion should have an even greater impact on solidification behavior than in LPBF. It appears far more likely that the shift in the cracking susceptibility curve to match the experimental data is due to rapid solidification and solute trapping increasing the partition coefficient.

CHAPTER 5 CONCLUSIONS

Binary Al-Cu alloy powders with 1.5, 3, 4.5, 6, and 10 wt.% were produced using gas atomization. These powders were used to create cuboidal samples using LPBF with 15 processing parameters for each composition. The microstructures of the samples in the XZ and XY planes were observed under an optical microscope and crack density analysis was conducted to measure the amount of solidification cracking in each sample. The crack density of the samples was examined as functions of energy density and compositions. For a fixed composition, the crack density mostly had an exponential decay relationship with energy density in which samples produced with high energy densities had far less cracking than samples built with high energy densities. Regardless of LPBF parameters employed, the crack density was the highest for the 3 and 4.5 wt.% Cu samples, and there was little cracking whatsoever for the 1.5 wt.% samples. From existing literature, it is known that Al-Cu alloys with ~1 wt.% Cu are the most susceptible to cracking for casting, while the laser melting of Al-Cu alloys tend to have the most solidification cracking around 3 - 4 Wt.% Cu. From the crack density analysis, the maximum crack density was approximated to be around 3.5 wt.% Cu.

Kou's cracking criteria, which has shown success in modeling solidification cracking susceptibility in cast alloys, was used to examine the cracking susceptibility of the manufactured alloys. When taking the partition coefficient at its equilibrium value and approximating the amount of solid-state back-diffusion using literature values for the solid-state diffusion coefficient, Kou's cracking criteria predicted a maximum cracking susceptibility at ~1 wt.% Cu. To shift the cracking susceptibility curve generated by Kou's cracking criteria to higher solute concentrations, the amount of back-diffusion needed to be increased above its literature value, or the partition

coefficient needed to be above its equilibrium value. The maximum values of α and k required to shift the cracking susceptibility curve to match the experimental data were calculated to be 0.175 and 0.46, respectively.

Furthermore, a parametric study was conducted to gain more insight into how these alter the cracking susceptibility curve in which was the back-diffusion Fourier number was varied along with the partition coefficient. Through this, it was found that the partition coefficient was more effective at shifting the cracking susceptibility curve towards higher solute concentrations, while increasing the Fourier number was more effective at lowering the magnitude of cracking susceptibility. A relationship between α and k was also developed that was required for the cracking susceptibility curve to match the experimental data.

Although both possible explanations were justifiable based on literature and solidification mechanics, the partition coefficient being above its equilibrium value seemed to be the primary factor in the discrepancy between Kou's solidification cracking model and the experimental findings. Solute trapping has been consistently observed in the manufacturing of Al-alloys in LPBF due to the processes' high cooling rates, which would increase the partition coefficient. The solid-liquid interface velocity required for sufficient solute trapping to increase the partition coefficient to 0.46 has been observed in the pulsed-laser melting of hypoeutectic Al-Cu, which has a comparable cooling rate to LPBF. Also, the fact that Kou was successful in modeling solidification cracking susceptibility in cast Al-Cu alloys while neglecting back-diffusion further suggests that increased back-diffusion is not as significant as the partition coefficient increasing for explaining the discrepancy between Kou's model and the experimental data for LPBF. Both explanations are possible, but it seems far more likely that rapid solidification and solute trapping

causing an increase in the partition coefficient is what caused the composition with the maximum cracking susceptibility to shift towards higher solute concentrations for LPBF.

CHAPTER 6 FUTURE WORK

While this thesis provides much insight into the solidification mechanics of LPBF manufactured alloys and is capable of suggesting why there is a discrepancy between Kou's cracking criteria and experimental findings, it falls short of adjusting Kou's model for solidification cracking so that it can be applied for other alloys. An equation was generated to solve for the partition coefficient in terms of the solid-liquid interface velocity for Al-Cu alloys, which would allow for Kou's model to accurately represent the cracking susceptibility of LPBF manufactured Al-Cu. However, there is still the need to find out the relationship between the solid-liquid interface velocity and the cooling rate. Future work done on this topic would be able to relate LPBF parameters to the partition coefficient, which would not only help predict which alloy compositions would be the most susceptible to cracking but allow for further control over the partition coefficient. Since the partition coefficient has a great impact on the composition at which the maximum cracking susceptibility occurs, understanding how the partition coefficient is impacted by processing parameters would allow for additional insight into which alloy compositions may be suitable for LPBF, i.e., alloy design. Furthermore, conducting this future work would quantify the partition coefficient for the alloys manufactured with LPBF, which would test my claim that the shift in the cracking susceptibility curve was mainly due to an increased partition coefficient. The quantification of the partition coefficient for LPBF manufactured Al-Cu alloys would strengthen the findings of the work reported in this thesis and developing an adjustment to Kou's solidification cracking model that would allow it to be used for alloy design specifically for LPBF and other additive manufacturing technologies.

REFERENCES

[1] Cobbinah, P.V., Nzeukou, R.A., Onawale, O.T., Matizamhuka, W.R., "Laser Powder Bed Fusion of Potential Superalloys: A Review", *Metals*, vol. 11, 58, 2021.

[2] Sindo Kou, "A criterion for cracking during solidification", *Acta Materialia*, vol. 88, pp. 366-374, 2015.

[3] Hyer, H., Zhou, L., Mehta, A. et al, "Effects of Alloy Composition and Solid-State Diffusion Kinetics on Powder Bed Fusion Cracking Susceptibility", *J. Phase Equilib. Diffus.*, 2020.

[4] Hyer, H., Zhou, L., Mehta, A. et al, "Composition-dependent solidification cracking of aluminum-silicon alloys during laser powder bed fusion", *Acta Materialia.*, vol. 208, 2021.

[5] Glicksman M.E., Rapid Solidification Processing, Principles of Solidification, *Springer*, New York, NY, 2011.

[6] Wang, Zhi et al. "Selective Laser Melting of Aluminum and Its Alloys." *Materials (Basel, Switzerland)*, vol. 13, 4564, 14 Oct. 2020.

[7] Sun, S., Brandt, M., & Easton, M., "Powder bed fusion processes", *Laser Additive Manufacturing*, pp. 55–77, 2017.

[8] Zhang, Y., Yang, S. & Zhao, Y.F., "Manufacturability analysis of metal laser-based powder bed fusion additive manufacturing—a survey", *Int J Adv Manuf Technol*, vol. 110, pp. 57–78, 2020.

[9] Khorasani, A., Gibson, I., Veetil, J. K., & Ghasemi, A. H, "A review of technological improvements in laser-based powder bed fusion of metal printers", *The International Journal of Advanced Manufacturing Technology*, 2020.

[10] Bosio, F., Aversa, A., Lorusso, M., Marola, S., Gianoglio, D., Battezzati, L. *et al*. "A time-saving and cost-effective method to process alloys by Laser Powder Bed Fusion", *Materials & Design*, 2019.

[11] Choo, H., Sham, K.-L., Bohling, J., Ngo, A., Xiao, X., Ren, Y., … Garlea, E., "Effect of laser power on defect, texture, and microstructure of a laser powder bed fusion processed 316L stainless steel", *Materials & Design*, 2018.

[12] Sola, A., Nouri, A., "Microstructural porosity in additive manufacturing: The formation and detection of pores in metal parts fabricated by powder bed fusion", *Journal of Advanced Manufacturing and Processing*, 2019.

[13] Mohanty, Upendra and Sarangi, Hrushikesh Solidification of Metals and Alloys, *IntechOpen*, Ch.2, 2021

[14] Grasso, M., and Colosimo, B. M., "Process defects and in situ monitoring methods in metal powder bed fusion: a review", *Measurement Science and Technology*, vol. 28, 2017.

[15] Aversa, A., Marchese, G., Saboori, A., Bassini, E., Manfredi, D., Biamino, S. *et al.* "New Aluminum Alloys Specifically Designed for Laser Powder Bed Fusion: A Review", *Materials*, vol. 12, (2019).

[16] Saket Thapliyal, Mageshwari Komarasamy, Shivakant Shukla, Le Zhou, Holden Hyer, Sharon Park, Yongho Sohn, Rajiv S. Mishra, "An integrated computational materials engineering-anchored closed-loop method for design of aluminum alloys for additive manufacturing", *Materialia*, vol. 9, 2020.

[17] A. K. Vasudevan, R. D. Doherty. *Aluminum Alloys--Contemporary Research and Applications*. Academic Press. vol. 31, pp. 50, 1989.

[18] Priyanka Agrawal, Sanya Gupta, Saket Thapliyal, Shivakant Shukla, Ravi Sankar Haridas, Rajiv S. Mishra, "Additively manufactured novel Al-Cu-Sc-Zr alloy: Microstructure and mechanical properties", *Additive Manufacturing*, vol. 37, 2021.

[19] Mair, P., Kaserer, L., Braun, J., Weinberger, N., Letofsky-Papst, I., & Leichtfried, G., "Microstructure and mechanical properties of a TiB2-modified Al–Cu alloy processed by laser powder-bed fusion", *Materials Science and Engineering: A*, 2020.

[20] Schmidtke, K., Palm, F., Hawkins, A., & Emmelmann, C., "Process and Mechanical Properties: Applicability of a Scandium modified Al-alloy for Laser Additive Manufacturing", *Physics Procedia*, vol. 12, pp. 369–374, 2011.

[21] Zhou, L., Hyer, H., Park, S., Pan, H., Bai, Y., Rice, K. P., & Sohn, Y., "Microstructure and mechanical properties of Zr-modified aluminum alloy 5083 manufactured by laser powder bed fusion", *Additive Manufacturing*, vol. 28, pp. 485–496, 2019.

[22] Mehta, A.,Zhou, L., Huynh, T., Park, S., Hyer, H., Song, S., Bai, Y., et al., "Additive manufacturing and mechanical properties of the dense and crack free Zr-modified aluminum alloy 6061 fabricated by the laser-powder bed fusion", *Additive Manufacturing*, vol. 41, 2021

[23] Sonawane, A., Roux, G., Blandin, J.-J., Despres, A., & Martin, G., "Cracking mechanism and its sensitivity to processing conditions during laser powder bed fusion of a structural Aluminum alloy", *Materialia*, 2020

[24] Zhou, L., Pan, H., Hyer, H., Park, S., Bai, Y., McWilliams, B., *et al*. "Microstructure and tensile property of a novel AlZnMgScZr alloy additively manufactured by gas atomization and laser powder bed fusion", *Scripta Materialia*, vol. 158, pp. 24–28, 2019.

[25] Flemings, M. C., “Solidification processing”, *Metallurgical Transactions*, vol. 5, pp. 2121–2134, 1974.

[26] Clyne, T. W., & Kurz, W., “Solute redistribution during solidification with rapid solid state diffusion”, *Metallurgical Transactions A*, vol. 12, pp. 965–971, 1981.

[27] Kobayashi, S., “A mathematical model for solute redistribution during dendritic solidification”, *Transactions of the Iron and Steel Institute of Japan*, vol. 28, pp. 535–542, 1988.

[28] Zhang, Jahazi, & Isabel Gallego. “On the Impact of Microsegregation Model on the Thermophysical and Solidification Behaviors of a Large Size Steel Ingot”, *Metals*, vol. 10, pp. 74, 2020.

[29] Hu, Z., Nie, X., Qi, Y., Zhang, H., & Zhu, H, “Cracking criterion for high strength Al–Cu alloys fabricated by selective laser melting”, *Additive Manufacturing*, 101709, 2020

[30] Qin, H., Dong, Q., Fallah, V., & Daymond, M. R. “Rapid Solidification and Non-equilibrium Phase Constitution in Laser Powder Bed Fusion (LPBF) of AlSi10Mg Alloy: Analysis of Nano-precipitates, Eutectic Phases, and Hardness Evolution”, *Metallurgical and Materials Transactions A*, 2019.

[31] Ghoncheh, M. H., Sanjari, M., Zoeram, A. S., Cyr, E., Amirkhiz, B. S., Lloyd, A., … Mohammadi, M., “On the Microstructure and Solidification Behavior of New Generation Additively Manufactured Al-Cu-Mg-Ag-Ti-B Alloys”, *Additive Manufacturing*, 2020.

[32] Kuhn, Howard and Lawley, Alan, “Powder Metallurgy Processing: The Techniques and Analyses”, *Academic Press*, 1978

[33] Sheikhi, M., Malek Ghaini, F., & Assadi, H., "Solidification crack initiation and propagation in pulsed laser welding of wrought heat treatable aluminium alloy", *Science and Technology of Welding and Joining*, vol. 19, pp. 250–255, 2014.

[34] Yan, X., & Lin, J. C., "Prediction of hot tearing tendency for multicomponent aluminum alloys", *Metallurgical and Materials Transactions B*, vol. 37, pp. 913–918, 2006.

[35] Tang, M., Pistorius, P. C., Narra, S., & Beuth, J. L., "Rapid Solidification: Selective Laser Melting of AlSi10Mg*", JOM*, vol. 68, pp. 960–966, 2016.

[36] Anyalebechi, Princewill, "Effects of alloying elements and solidification conditions on secondary dendrite arm spacing in aluminum alloys", *TMS Annual Meeting*, pp. 217-233, 2004.

[37] E.A. Brandes, G.B. Brook, Smithells Metals Reference Book, Seventh Edition, Butterworth-Heinemann, 1992

[38] Ceotto, Diego & Miani, Fabio, "Empirical model for the estimation of thermophysical properties of liquid metal alloys", *High Temperature*, vol. 52, pp. 385-389, 2014.

[39] Mauduit, Arnold, "Study of the suitability of aluminum alloys for additive manufacturing by laser powder bed fusion", *UPB Scientific Bulletin, Series B: Chemistry and Materials Science*, vol. 79, pp. 219–238, 2017.

[40] Smith, P. M., & Aziz, M. J., "Solute trapping in aluminum alloys", Acta Metallurgica et Materialia, vol. 42, pp. 3515–3525, 1994

[41] M. J. Aziz and T. Kaplan, "Continuous growth model for interface motion during alloy solidification", *Acta Metallurgica*, vol. 36, pp. 2335-2347, 1988.

[42] McKeown, J. T. et al., “In situ transmission electron microscopy of crystal growth-mode transitions during rapid solidification of a hypoeutectic Al–Cu alloy”, Acta Materialia, vol. 65, pp. 56–68, 2014.